

**Repository of the Max Delbrück Center for Molecular Medicine (MDC)
in the Helmholtz Association**

<http://edoc.mdc-berlin.de/20959/>

**Propionate attenuates atherosclerosis by immune-dependent regulation
of intestinal cholesterol metabolism**

Haghikia A., Zimmermann F., Schumann P., Jasina A., Roessler J., Schmidt D., Heinze P., Kaisler J., Nageswaran V., Aigner A., Ceglarek U., Cineus R., Hegazy A.N., van der Vorst E.P.C., Döring Y., Strauch C.M., Nemet I., Tremaroli V., Dwibedi C., Kränkel N., Leistner D.M., Heimesaat M.M., Bereswill S., Rauch G., Seeland U., Soehnlein O., Müller D.N., Gold R., Bäckhed F., Hazen S.L., Haghikia A., Landmesser U.

This is the final version of the accepted manuscript.

This is a pre-copyedited, author-produced PDF of an article accepted for publication in European Heart Journal following peer review. The version of record

Arash Haghikia and others, Propionate attenuates atherosclerosis by immune-dependent regulation of intestinal cholesterol metabolism, European Heart Journal, Volume 43, Issue 6, 7 February 2022, Pages 518–533.

is available online at <https://academic.oup.com/eurheartj/article/43/6/518/6379035> or
<https://doi.org/10.1093/eurheartj/ehab644>.

European Heart Journal
2022 FEB 07 ; 43(6): ehab644
2021 OCT 01 (first published online: final publication)
doi: [10.1093/eurheartj/ehab644](https://doi.org/10.1093/eurheartj/ehab644)

Publisher: [Oxford University Press](#)

Copyright © The Author(s) 2021.

Propionate attenuates atherosclerosis by immune-dependent regulation of intestinal cholesterol metabolism

Arash Haghikia^{1,2,3#}, Friederike Zimmermann^{1,2}, Paul Schumann^{1,2}, Andrzej Jasina¹, Johann Roessler^{1,2}, David Schmidt¹, Philipp Heinze¹, Johannes Kaisler⁴, Vanasa Nageswaran¹, Annette Aigner^{3,5}, Uta Ceglarek^{6,7}, Roodline Cineus^{8,9}, Ahmed N. Hegazy^{3,8,9}, Emiel P.C. van der Vorst^{10,11,12,13}, Yvonne Döring^{10,11,14}, Christopher M. Strauch¹⁵, Ina Nemet¹⁵, Valentina Tremaroli¹⁶, Chinmay Dwibedi^{16,17}, Nicolle Kränkel^{1,2}, David M. Leistner^{1,2,3}, Markus M. Heimesaat¹⁸, Stefan Bereswill¹⁸, Geraldine Rauch^{3,5}, Ute Seeland^{2,19}, Oliver Soehnlein^{10,11,20}, Dominik N. Müller^{2,3,21,22}, Ralf Gold⁴, Fredrik Bäckhed^{16,23,24}, Stanley L. Hazen^{15,25}, Aiden Haghikia^{26*}, Ulf Landmesser^{1,2,3*}

*Authors contributed equally as senior authors.

¹Department of Cardiology, Charité-Universitätsmedizin Berlin, Campus Benjamin Franklin, Berlin, Germany

²German Center for Cardiovascular Research (DZHK), Partner Site Berlin, Berlin, Germany

³Berlin Institute of Health (BIH), Berlin, Germany

⁴Department of Neurology, St. Josef-Hospital, Ruhr-University Bochum, Bochum, Germany

⁵Institute of Biometry and Clinical Epidemiology, Charité - Universitätsmedizin Berlin, Germany

⁶Institute of Laboratory Medicine, Clinical Chemistry and Molecular Diagnostics, University Hospital Leipzig, Germany

⁷LIFE-Leipzig Research Center for Civilization Diseases, University of Leipzig, Germany.

⁸Department of Gastroenterology, Infectiology, and Rheumatology, Charité-Universitätsmedizin Berlin, Campus Benjamin Franklin, Berlin, Germany

⁹Deutsches Rheumaforschungszentrum Berlin (DRFZ), An Institute of the Leibniz Association

¹⁰Institute for Cardiovascular Prevention (IPEK), LMU München, Munich, Germany

¹¹German Center for Cardiovascular Research (DZHK), Partner Site Munich, Heart Alliance Munich, Germany

¹²Interdisciplinary Center for Clinical Research (IZKF), Institute for Molecular Cardiovascular Research (IMCAR), RWTH Aachen University, Aachen, Germany

¹³Department of Pathology, Cardiovascular Research Institute Maastricht (CARIM), Maastricht University, Maastricht, the Netherlands

¹⁴Department of Angiology, Swiss Cardiovascular Center, Inselspital, Bern University Hospital, University of Bern, Switzerland

¹⁵Department of Cardiovascular & Metabolic Sciences, Lerner Research Institute, Cleveland Clinic, Cleveland, OH 44106, USA

¹⁶The Wallenberg Laboratory, Department of Molecular and Clinical Medicine, Institute of Medicine, Sahlgrenska Academy, University of Gothenburg, Gothenburg, Sweden

¹⁷Institute of Neuroscience and Physiology, University of Gothenburg, Sweden

¹⁸Institute of Microbiology, Infectious Diseases and Immunology, Charité-Universitätsmedizin Berlin, Berlin, Germany

¹⁹Charité - Universitätsmedizin Berlin, corporate member of Freie Universität Berlin, Humboldt-Universität zu Berlin, and Berlin Institute of Health; Institute of Social Medicine, Epidemiology and Health Economics, Berlin, Germany

²⁰Institute for Experimental Pathology (ExPat), Center for Molecular Biology of Inflammation (ZMBE), WWU Münster, Germany

²¹Experimental and Clinical Research Center, a joint cooperation of Max Delbrück Center for Molecular Medicine and Charité-Universitätsmedizin Berlin, Berlin, Germany

²²Max Delbrück Center for Molecular Medicine in the Helmholtz Association, Berlin, Germany

²³Novo Nordisk Foundation Center for Basic Metabolic Research, Faculty of Health and Medical Sciences, University of Copenhagen, Denmark

²⁴Region Västra Götaland, Sahlgrenska University Hospital, Department of Clinical Physiology, Gothenburg, Sweden.

²⁵Department of Cardiovascular Medicine, Heart and Vascular Institute, Cleveland Clinic, Cleveland, Ohio, USA

²⁶Department of Neurology, Otto-von-Guericke University, Magdeburg, Germany

#Corresponding author:

Arash Haghikia, MD

Department of Cardiology

Charité-Universitätsmedizin Berlin

Campus Benjamin Franklin

Hindenburgdamm 30

12203 Berlin, Germany

Phone: +49 30 450 513 638

Fax: + 49 30 450 513 996

E-mail: arash.haghikia@charite.de

Abstract

Aims: Atherosclerotic cardiovascular disease (ACVD) is a major cause of mortality and morbidity worldwide, and increased low-density lipoproteins (LDL) play a critical role in development and progression of atherosclerosis. Here we examined for the first time gut immunomodulatory effects of the microbiota-derived metabolite propionic acid (PA) on intestinal cholesterol metabolism.

Methods and results:

Using both human and animal model studies, we demonstrate that treatment with PA reduces blood total and LDL cholesterol levels. In apolipoprotein E^{-/-} (*ApoE*^{-/-}) mice fed a high-fat diet (HFD) PA reduced intestinal cholesterol absorption and aortic atherosclerotic lesion area. Further, PA increased regulatory T cell numbers and interleukin (IL)-10 levels in the intestinal microenvironment, which in turn suppressed the expression of Niemann-Pick C1-like 1 (*Npc1l1*), a major intestinal cholesterol transporter.

Blockade of IL-10 receptor signaling attenuated the PA-related reduction in total and LDL cholesterol and augmented atherosclerotic lesion severity in the HFD-fed *ApoE*^{-/-} mice.

To translate these preclinical findings to humans, we conducted a randomized, double-blinded, placebo-controlled human study (clinical trial No. NCT03590496). Oral supplementation with 500 mg of PA twice daily over the course of 8 weeks significantly reduced LDL [-15.9 mg/dl (-8.1%) vs -1.6 mg/dl (-0.5%), *P* = 0.016], total [-19.6 mg/dl (-7.3%) vs -5.3 mg/dl (-1.7%), *P* = 0.014] and Non-HDL cholesterol levels [PA vs placebo: -18.9 mg/dl (-9.1%) vs -0.6 mg/dl (-0.5%), *P* = 0.002] in subjects with elevated baseline LDL cholesterol levels.

Conclusion: Our findings reveal a novel immune-mediated pathway linking the gut microbiota-derived metabolite PA with intestinal *Npc1l1* expression and cholesterol homeostasis. The results highlight the gut immune system as a potential therapeutic target to control dyslipidemia, that may introduce a new avenue for prevention of atherosclerotic cardiovascular diseases.

Introduction:

Atherosclerotic cardiovascular diseases (ACVDs) are a major global health care burden and a leading cause of mortality and morbidity worldwide ¹. Elevated levels of low-density lipoprotein (LDL) and non-high-density lipoprotein (non-HDL) cholesterol are important modifiable risk factors for ACVD, thus representing a major effective target for ACVD prevention ^{2,3}. In recent years, increasing attention has been devoted to identifying gut microbial pathways affecting metabolic pathways ⁴ or atherogenesis ⁵⁻⁷. In particular, gut microbiota-derived metabolites that are transported to the peripheral circulation in the host via the portal vein can act as signaling molecules and may impact atherogenesis by regulating host metabolism ⁸, immune homeostasis ⁹, and vascular function ^{10,11}.

Among detrimental metabolites, trimethylamine N-oxide (TMAO), generated by gut microbial metabolism of trimethylamine-containing nutrients such as choline and carnitine, has been shown to promote the development of atherosclerosis in animal models ^{5,6,12} with prognostic implications for patients with coronary heart disease ¹³, chronic kidney disease ¹⁴, ischaemic stroke ¹⁵, and mortality ¹⁶. Short-chain fatty acids (SCFAs; i.e. acetic, propionic, and butyric acids) derived by gut microbial fermentation of dietary fibres, on the other hand, have shown beneficial effects on host metabolism and cardiac health ^{17,18}. Although SCFAs are primarily considered important energy sources in intestinal epithelial cells, they also possess regulatory properties and affect host metabolism, immune homeostasis and cell proliferation ¹⁷. Propionic acid (PA) has been shown to critically regulate T cell-mediated immunity and thereby modulate the disease course in autoimmune diseases, particularly by promoting the differentiation and functional capacity of CD25⁺ Foxp3⁺ regulatory T cells (Tregs)¹⁹⁻²¹. PA also has been reported to promote beneficial effects on cardiac remodelling in experimental hypertension by counteracting hypertension-induced imbalance between Tregs and effector T cells ²². Epidemiological studies suggest that sufficient fibre intake may contribute to preventing dyslipidemia and atherosclerotic vascular disease ²³. However, the underlying mechanisms remain unclear. Tregs have been reported to have the ability to modulate cholesterol metabolism and subsequent atheroprotective effects ²⁴, which raises the question of whether SCFAs may regulate lipids in an immune-dependent way.

Here, we examine for the first time pathways whereby the microbiome-derived short chain fatty acid PA may regulate lipoprotein levels, that are causal for atherosclerotic lesion development in hypercholesterolemic and atherosclerosis-prone apolipoprotein E (*ApoE*)^{-/-} mice. Moreover, in a proof-of-concept double-blind and placebo-controlled clinical study, the effect of PA on LDL and total cholesterol levels was evaluated in humans with hypercholesterolemia.

Results:

Short-chain fatty acid propionate prevents HFD-induced hypercholesterolemia and atherosclerosis in *Apoe*^{-/-} mice

We first evaluated gut microbiota-dependent control of plasma lipids using conventionally raised and antibiotic treated *Apoe*^{-/-} mice (ABS) with a depleted gut microbiota that were fed either a standard chow (SCD) or high-fat diet (HFD) for 6 weeks. In mice with a depleted gut microbiota, we found increased levels of total (TC), very low-density lipoprotein (VLDL) and LDL cholesterol compared to those of conventionally (CONV) raised *Apoe*^{-/-} mice under a SCD and a HFD (*Figure 1A - F*). These findings support a functional role of gut microbiota-dependent metabolic pathways in the control of blood cholesterol levels. The increase in cholesterol levels was accompanied by increased atherosclerotic lesion size after 6 weeks of either diet (*Figure 1G,H*). Next, we examined the effect of exogenous PA administered via daily oral gavage on plasma lipids in hypercholesterolemic *Apoe*^{-/-} mice (*Figure 2A*). We observed that treatment with PA (200 mg/kg) prevented HFD-induced increases in total, VLDL, and LDL cholesterol (*Figure 2B,F*).

Importantly, the vehicle used for oral gavage (0.9% sodium chloride) did not have any relevant effects on blood lipids metabolism (*Suppl Figure S1*). Moreover, HFD increased several cholesteryl esters, some of which were reduced upon treatment with PA (*Suppl Figure S2*). Consequently, the HFD-induced increase in atherosclerotic lesion size was attenuated by PA (*Figure 2G,H*).

Notably, PA treatment significantly lowered total, LDL and VLDL cholesterol in antibiotic treated and HFD-fed *Apoe*^{-/-} mice (*Suppl Figure S3A-E*) demonstrating that PA can compensate for the de-regulated intestinal cholesterol metabolism in gut microbiota depleted mice. Treatment with PA also tended to attenuate atherosclerotic lesion size in antibiotic treated and HFD-fed *Apoe*^{-/-} mice, although this effect did not reach statistical significance (*Suppl Figure S3F,G*) suggesting that gut microbial dependent anti-atherogenic mechanisms go beyond intestinal cholesterol regulation.

Propionate impacts intestinal cholesterol metabolism by modulating the expression of Niemann-Pick C1-like protein 1

To further understand the mechanisms underlying PA-mediated lipid regulation, we determined the expression of major genes involved in hepatic cholesterol metabolism. We found upregulated expression of sterol regulatory element-binding protein (*Srebp2*) and cholesterol 7 alpha-hydroxylase (*Cyp7a1*) in hypercholesterolemic *Apoe*^{-/-} mice, of which only the upregulated expression of *Srebp2* was reversed upon PA treatment (*Figure 3A,B*). Other genes involved in hepatic cholesterol and bile acid synthesis, including LDL receptor (*Ldlr*)

(Figure 3C), proprotein convertase subtilisin/kexin type 9 (*Pcsk9*), 3-hydroxy-3-methyl-glutaryl-coenzyme A (HMG-CoA) reductase (*Hmgcr*), and farnesoid X receptor (*Fxr*), were not significantly altered by HFD or additional PA treatment (*Suppl Figure S4A-C*). Next, we sought to investigate whether PA impacts the activity of HMG-CoA reductase, the rate-controlling enzyme of cholesterol synthesis. However, the enzymatic activity of HMG-CoA reductase was not affected by PA at increasing concentrations (*Suppl Figure S4D*). These findings argue against a relevant role of PA in hepatic regulation of cholesterol metabolism. In addition to hepatic cholesterol clearance and synthesis, intestinal cholesterol metabolism, particularly cholesterol trafficking and absorption, are key components of cholesterol homeostasis²⁵. We therefore investigated a potential regulatory role of PA on intestinal expression of Niemann-Pick C1-like protein 1 (*Npc1l1*), a major transmembrane transporter responsible for intestinal cholesterol absorption²⁶. We also examined the impact of PA on the expression of apical sodium–bile acid transporter (*Asbt*), which mediates active uptake of conjugated bile acids²⁷ to maintain their enterohepatic recirculation. While PA normalized the HFD-induced increase in *Npc1l1* gene expression in the small intestine, it did not affect HFD-induced *Asbt* expression (*Figure 3D,E*). Increased density of NPC1L1 was also observed in histological sections of the small intestine from *Apoe*^{-/-} mice fed with HFD compared to mice fed with SCD and was prevented in HFD-fed mice under PA treatment (*Figure 3F,G*). Interestingly, we found no significant differences in the expression of genes regulating the flux of lipids across small intestinal enterocytes, including ATP-binding cassette subfamily G member 5 (*Abcg5*), acetyl-CoA acetyltransferase (*Acat2*) and ATP-binding cassette transporter 1 (*Abca1*), between PA-treated and untreated mice (*Suppl Figure 5A-C*). Next, we investigated the functional relevance of altered *Npc1l1* expression and analyzed plasma levels of the phytosterols stigmasterol and sitosterol in *Apoe*^{-/-} mice that were fed with SCD or HFD with or without PA. Since the abundance of plasma phytosterol depends on dietary intake and intestinal sterol absorption capacity, plasma levels of phytosterols serve as an indicator of the intestinal sterol absorption rate²⁸. We found increased levels of both stigmasterol and sitosterol in mice fed with HFD, and this change was prevented upon treatment with PA (*Figure 3H,I*). Moreover, we found increased levels of fecal cholesterol in HFD fed mice treated with PA as compared to mice without PA treatment (*Suppl Figure S6*). These observations suggested that PA modulates intestinal sterol absorption capacity, which is in line with the observed downregulation of *Npc1l1* by PA. We used a mouse intestinal epithelial organoid culture system after specific expansion of adult intestinal stem cells²⁹ to examine the regulatory role of PA in modulating *Npc1l1*. Interestingly, treatment of the intestinal organoids with different concentrations of PA revealed no significant effect of PA on the expression of the *Npc1l1* gene (*Suppl Figure S7*), suggesting a more complex regulation of *Npc1l1* by PA.

Treatment with propionate increases Tregs and IL-10 in the small intestine

In view of recent insights into the modulatory effects of PA on intestinal T cell immunity^{20,30}, and growing evidence for the involvement of intestinal T cells in the control of systemic metabolism³¹, we hypothesized that modulation of the intestinal adaptive immune system at least partly mediates PA-related alterations in cholesterol metabolism. In line with previous reports^{20,30} we observed an increase of CD25⁺Foxp3⁺Tregs in the mesenteric lymph nodes (MLNs) and the peripheral circulation (*Figure 4A-C*) of HFD-fed *ApoE*^{-/-} mice in response to PA. Notably, the splenic Treg population was not altered, suggesting that the small intestine was the primary source of the increase in Tregs in response to PA in our model (*Figure 4D*). Notably, we did not observe alterations in T helper 1 (Th1) or Th17 cell frequencies in the MLNs, peripheral circulation or spleen upon PA treatment (*Suppl Figure S8A-F*). The increase in the Treg cell population in response to PA was accompanied by increased concentrations of interleukin (IL)-10, the major Treg-cytokine, in the small intestinal wall (*Figure 4E*). Other cytokines related to T helper 1 (Th1) or Th17 cells or monocytes, including tumour necrosis factor-alpha (TNF- α), monocyte chemoattractant protein-1 (MCP-1), IL-6, and interferon gamma (IFN- γ), were not altered by PA (*Figure 4F-I*).

IL-10 regulates the intestinal expression of Niemann-Pick C1-like protein 1

To examine potential regulation of the *Npc1l1* gene by IL-10, we used mouse intestinal epithelial organoids (*Figure 5A*), which express both the IL-10R1 and IL-10R2 receptor³² (*Figure 5B*). Treatment with recombinant mouse IL-10 induced dose-dependent downregulation of *Npc1l1* gene expression (*Figure 5C*). To further explore the functional relevance of IL-10-dependent regulation of *Npc1l1* gene expression for PA-related intestinal cholesterol metabolism and atheroprotection, we blocked IL-10 signaling using an anti-IL-10 receptor monoclonal antibody (AB), which was intraperitoneally injected once per week during the PA treatment period (*Figure 5D*). Blockade of IL-10 receptor signaling attenuated the PA-related lowering effect on total, LDL, VLDL, and HDL cholesterol (*Figure 5E-I*) and augmented atherosclerotic lesion severity in HFD-fed *ApoE*^{-/-} mice (*Figure 5J,K*). Notably, inhibition of IL-10 receptor signaling resulted in elevated phytosterol plasma levels (*Figure 5L- M*), which is indicative of enhanced intestinal sterol absorption.

These findings support a regulatory circuit in which PA-induced elevations of Treg cell frequency and local IL-10 concentrations in the small intestine regulate the expression of the major sterol transporter NPC1L1. Thereby, PA indirectly regulates the absorption of cholesterol, with subsequent implications for the development of hyperlipidemia-induced atherosclerosis in *ApoE*^{-/-} mice.

PA reduces serum LDL and total cholesterol in hypercholesterolemic humans

To explore the clinical relevance of our findings, we performed a randomized, double-blind and placebo-controlled study in hypercholesterolemic subjects evaluating the effect of oral supplementation of PA on LDL cholesterol blood levels as a primary end point and total, non-HDL and HDL cholesterol levels among the secondary end points (trial profile shown in *Suppl Figure S9*). A total of 62 individuals with baseline LDL cholesterol levels > 115 mg/dl were enrolled and underwent 1:1 randomization to receive either oral placebo (500 mg) twice daily or PA (500 mg) twice daily for 8 weeks. The baseline clinical characteristics and biochemical parameters did not differ between the two study groups (Table 1). Study participants were advised to maintain their regular physical activity and dietary habits during the study period (dietary information shown in *Suppl Table S1*).

After 8 weeks, PA lowered LDL cholesterol levels [PA vs placebo: -15.9 mg/dl (-8.1%) vs -1.6 mg/dl (-0.5%), $P = 0.016$] and total cholesterol levels [PA vs placebo -19.6 mg/dl (-7.3%) vs -5.3 mg/dl (-1.7%), $P = 0.014$] compared to placebo (*Figure 6A-D*). Moreover, PA also lowered non-HDL cholesterol levels [PA vs placebo: -18.9 mg/dl (-9.1%) vs -0.6 mg/dl (-0.5%), $P = 0.002$], whereas no significant difference in the change in HDL cholesterol levels [PA vs placebo: -0.7 mg/dl (-0.9%) vs -4.7 mg/dl (-6.0%), $P = 0.078$] was observed between the groups (*Figure 6E-H*). Notably, since the majority of study participant is represented by women (Table 1), in a subanalysis we evaluated the change in LDL and total cholesterol levels in male study participants and found a significant reduction in LDL [difference between: Mean (95% CI): -15.75 (-31.31; -0.18); $P = 0.048$] as well as in total cholesterol [difference between: Mean (95% CI): -23.12 (-41.45; -4.79); $P = 0.018$] upon PA supplementation as compared to placebo pointing to a sex-independent cholesterol lowering effect of PA. No significant difference was observed for the change in body weight (*Figure 7A,B*). The safety and tolerability parameters were similar between the placebo and PA groups (Table 2), with no PA-related severe adverse events (for complete analysis of study results see Supplementary File). Oral supplementation of PA led to a significant intra-individual increase of PA concentration in the plasma after 8 weeks (*Suppl Figure S10A*) but did not affect gut microbiota composition and diversity in a subset of participants for whom faecal samples were available at baseline and at the end of the study (*Suppl Figure S10B-C*). In line with the finding from the experimental studies, phenotyping of peripheral T cells displayed significant increase of Tregs in the PA group (*Suppl Figure S11A,B*) without significant alteration of Th17 or Th1 cell numbers (*Suppl Figure S12A,B*).

Moreover, we evaluated the effect of PA on plasma levels of two distinct factors, fatty acid-binding protein 4 (FABP4) and glucagon, involved in the regulation of glucose metabolism, which were not significantly altered upon oral supplementation with PA (*Suppl Figure S13*).

Discussion:

Despite previous studies implicating atheroprotective effects of the short chain fatty acid (SCFA) propionate (PA) ^{22,33}, this is the first study demonstrating the regulatory property of propionate to decrease intestinal cholesterol absorbance via an immunomodulatory pathway. This pathway involves a novel circuit in which increased IL-10 in the intestinal microenvironment downregulates NPC111, the major intestinal cholesterol transporter. Moreover, the clinical relevance of the experimental observations is highlighted for the first time in a randomized, placebo-controlled, double-blind trial evaluating the cholesterol-lowering effect of propionate demonstrating the translational potential of our findings.

Bartolomaeus et al.²² showed vasoprotective effects of PA in a mouse model of angiotensin II induced hypertensive cardiovascular damage, e.g. by preventing angiotensin II- induced local cardiac proinflammatory immune cell infiltration. Other vasoprotective properties of propionate include blood pressure lowering effects in mice via endothelial G protein-coupled receptor by dilating resistance vessels in an endothelium-dependent manner¹⁰. While in these studies lipid-independent models of vascular pathologies were used, our study focused on lipid-modulating properties of PA with subsequent protective effects on atherosclerosis development.

Gut microbial-generated metabolites are important modulators of the host physiologic functions and metabolism ³⁴. SCFAs are derived from anaerobic fermentation of undigested nutrients such as dietary fiber and complex polysaccharides and are considered to have health-promoting properties, e.g. by lowering blood pressure ^{10,18} and modulating inflammatory responses ²⁰. Moreover, epidemiological studies have suggested that long-term fiber intake may contribute to preventing dyslipidemia and atherosclerotic vascular disease ²³, although the underlying mechanisms are only poorly understood.

The current study demonstrates a marked increase in total and LDL cholesterol levels with an increased atherosclerotic lesion size in *Apoe*^{-/-} mice with antibiotic-induced depletion of the gut microbiota as compared to conventionally raised *Apoe*^{-/-} mice. These findings support a functional role of gut microbiota-dependent metabolic pathways in the control of blood cholesterol levels and atherogenesis. In particular, we show here that the SCFA propionate (PA) regulates intestinal expression of the intestinal cholesterol transporter of Niemann-Pick C1-like 1 (NPC1L1) by increasing IL-10 levels in the intestinal microenvironment. Thereby, PA controls circulatory LDL cholesterol levels and attenuates the development of atherosclerosis. The clinical relevance of our experimental findings was demonstrated in a double-blind, placebo-controlled proof-of-concept trial validating the LDL-cholesterol lowering effect of oral supplementation of propionate in hypercholesterolemic human subjects. Thus, lowering LDL cholesterol with potential atheroprotective effects by supplementary PA treatment may represent a novel application of a microbiota-derived metabolite. However, further studies are required to evaluate long-term effects of PA on the development of atherosclerosis in humans.

Atherosclerotic cardiovascular diseases (ACVDs) are a major global health care burden and a leading cause of mortality and morbidity worldwide ¹. Atherosclerosis starts frequently early in life ³⁵, and further progresses resulting in clinical ACVDs depending on lifetime exposure to both genetic and environmental causal risk factors ³⁶. Extensive evidence from epidemiologic, genetic, and clinical intervention studies has shown that LDL is causal in this process ³⁷. Thus, lowering LDL cholesterol levels is a cornerstone in prevention of the development and progression of ACVDs ².

In addition to traditional cardiovascular risk factors, in recent years, distinct changes in gut microbial composition have been described in the setting of atherosclerotic CVD in a number of case-controlled studies ³⁴. A large metagenome-wide association study on stools from individuals with atherosclerotic CVD and healthy controls demonstrated an increased abundance of *Enterobacteriaceae* and *Streptococcus spp.* and relatively depleted butyrate and propionate-producing bacteria in patients with atherosclerotic CVD, suggesting a functional role of SCFAs in promoting cardiovascular health ³⁸. In the vasculature propionate was demonstrated to mediate vasodilating effects by activating the G-protein-coupled receptor 41 in the vascular endothelium and thereby lower blood pressure ¹⁰.

In recent experimental studies, PA was shown to promote the repair capacity after myocardial infarction ³⁹ and protect against hypertensive and ischemic cardiac injury ²² by maintaining immune homeostasis. Although the underlying mechanisms are not fully understood, intestinal and systemic immune modulation appear to contribute to PA-related cardioprotection. Our observations expand on the recently reported immunomodulatory effects of propionate in the small intestine ^{20,21} and link the immune-regulatory elements with intestinal lipid control. Our findings reveal a novel regulatory circuit in which PA-induced increases in IL-10, the key Treg cytokine, in the intestinal microenvironment suppress small intestinal NPC1L1 expression, which in turn decreases intestinal cholesterol absorption. Consequently, the resulting decrease in circulatory LDL cholesterol levels attenuates the progression of atherosclerosis in hypercholesterolemic *ApoE*^{-/-} mice. This hypothesis is further supported by the reversal of the PA-induced effects on cholesterol control and atherosclerosis upon blockade of IL-10 receptor signaling, demonstrating that the underlying mechanism relies on IL-10 signaling in intestinal epithelial cells. Notably, the intestinal immune system, specifically distinct subsets (integrin $\beta 7^+$) of gut intraepithelial T lymphocytes, has been recently recognized to modulate systemic metabolism, including circulating cholesterol levels ³¹. Our findings support the notion that the intestinal immune cell compartment may serve as a novel target to control lipid metabolism. Our observations align with previous studies showing an increase in Treg number and function by supplementary PA treatment ²¹. Mechanistically, it was shown that PA augments the functional capacity of Tregs with increased IL-10 production by enhancing mitochondrial respiration. Moreover, *ex-vivo* transcriptome and network connectivity analyses in peripheral

blood cells from PA-treated subjects revealed upregulation of T cell receptor associated genes such as CD3 ϵ and CD28 in combination with key cofactors in T cell activation, such as IL-2 receptor alpha chain (IL2RA), with IL-10 as one of the major gene interaction hubs ²¹.

Importantly, a cholesterol-lowering effect has been attributed to IL-10 in clinical studies testing recombinant human IL-10, e.g., in autoimmune and neoplastic diseases ^{40,41} However, the underlying pathway of IL-10-mediated regulation of lipid metabolism remains unclear. Our findings reveal a novel regulatory role of IL-10 in intestinal cholesterol absorption by impacting the expression of NPC1L1. Importantly, unlike systemic immunotherapy with recombinant IL-10, local enrichment of IL-10 in the intestinal microenvironment by supplementary PA treatment may prevent adverse side-effects while promoting cardiovascular health and atheroprotection.

Notably, PA has been recently reported to stimulate glycogenolysis and hyperglycemia by increasing plasma concentrations of glucagon and fatty acid-binding protein 4 (FABP4) through activation of the sympathetic nervous system thereby increasing the risk of insulin resistance ⁴². Notably, in our study PA did not affect plasma concentrations of glucagon nor fatty acid-binding protein 4 (FABP4). These results together with unaltered fasting glucose and HbA1C levels under PA treatment suggest that PA treatment with the dosage and duration used in our study does not affect glucose metabolism. The SCFAs PA and butyrate have also been shown in previous studies to activate intestinal gluconeogenesis via a gut-brain neural circuit involving the fatty acid receptor FFAR3 ⁴³. However, this mechanism was suggested to rather promote metabolic benefits in energy homeostasis with reduced adiposity and body weight and better glucose control, including a decrease of hepatic glucose production. Taken together, PA may have diverse effects on glucose control depending on the site of action. Notably, in the current study many of the study participants from both groups were obese. However, we did not observe any relevant weight alteration in human study participants after 8 weeks PA treatment. This finding may indicate that in humans the cholesterol lowering property of PA, at least in the short-term, is not coupled with weight reduction.

Thus, further long-term studies are warranted to address the long-term metabolic effects of supplementary PA treatment examining glucose, cholesterol, and weight control.

Beyond the atheroprotective role of PA, future studies should evaluate the effects of distinct SCFA on hepatic steatosis and a broader analyses of hepatic signaling involved in SCFA dependent cholesterol metabolism and synthesis should require more attention.

In conclusion, our observations suggest a novel mechanism linking propionate-mediated effects on the gut immune system to intestinal cholesterol regulation, through which exogenous propionate modulates intestinal cholesterol absorption, thereby lowering blood LDL and total cholesterol levels. The clinical relevance of our experimental observations was demonstrated in a proof-of-concept clinical study highlighting the gut immune system as a potential therapeutic target for cardiovascular prevention in humans. Augmentation of intestinal

propionate, e.g., by oral supplementation or diet-based strategies, may provide a novel approach to modulate the intestinal immune system and thereby promote cardiovascular health and prevent atherosclerotic CVD. Further studies are needed to evaluate its long-term metabolic effects and consequences on cardiovascular outcome.

Limitations of the study:

A potential limitation of the clinical study is the rather short duration of PA treatment of 8 weeks. Thus, it cannot be ruled out that PA-mediated effects may be counteracted by potential negative feedback mechanisms upon long-term application. This needs to be further examined in future studies. Furthermore, the experimental findings were obtained using female mice, and in the clinical trial the majority is represented by women. However, in a subanalysis of our study cohort we observed a significant cholesterol lowering effect also in male study participants upon treatment with PA indicating that the effects are sex-independent. Nevertheless, the sex-independent cholesterol lowering effects of PA remain to be further confirmed in larger studies.

Although we did not find an alteration in the gut microbial profile upon treatment with PA, it cannot be excluded that the metabolic activity and functional property of distinct bacterial species may be altered in response to oral application of PA and, at least partly, contribute to the lipid-regulatory effects of PA, since distinct bacterial strains, such as *Lactobacillus* strains, known to metabolize propionate, have also cholesterol-lowering properties⁵⁸.

Materials and Methods

Mouse experiments

All animals were bred, raised, and housed in the “Forschungseinrichtungen für Experimentelle Medizin” (FEM, Charité – University Medicine Berlin, Germany) facilities under specific pathogen-free (SPF) conditions. All experiments were in accordance with the German/European law for animal protection and were approved by the local ethics committee (Das Landesamt für Gesundheit und Soziales Berlin, G0295/16). Animal numbers were calculated with nQuery + nTerim 4.0 software. A two-tailed test with a significance levels (α) of 0.05 and a power of 80% was considered with an estimated effect size from our previous work based on the effect of propionate on intestinal regulatory T-cells²⁰. The mice were maintained on a 12:12 h day:night cycle with constant access to food and water. Adult (16 weeks of age) female C57BL/6J, *Apoe*^{-/-} (Charles River) were age-matched and randomly assigned to either a standard chow diet (SCD, n=12) (crude fat 4.1%, cholesterol 14 mg/kg; Ssniff, Soest, Germany, E15000) or a high-fat diet (HFD, n=23) (crude fat 34.6%, cholesterol 290 mg/kg; Ssniff, Soest, Germany, E1574) for a total of 6 weeks. To study the effect of propionate (PA), calcium propionate (150 mM, Sigma-Aldrich) was administered daily via oral gavage for 4 weeks starting after 2 weeks of HFD (HFD+PA, n=13). Administration of SCFAs by oral gavage has been shown to effectively increase plasma SCFA levels⁴⁴. The mice that were not treated with PA received the vehicle (0.9% sodium chloride) alone (n=10). Inhibition of IL-10 receptor signaling during the period of PA treatment was achieved by intraperitoneal injection of an anti-IL-10 receptor monoclonal antibody (clone 1B1.2, 1mg per mouse per week, n=8) for 4 weeks starting at the end of week 2. All mice were sacrificed at the end of week 6 for the collection of blood and organs. Measured values were excluded in cases of technical failure during the experiment or by statistical testing, as described below. The exact mouse numbers are shown in the respective figures.

Generation of secondary abiotic mice

To generate secondary abiotic mice, quintuple antibiotic treatment (+ABS) was applied for 6 weeks. For this, mice were transferred to sterile cages and treated with a mixture of ampicillin plus sulbactam (1 g/L), vancomycin (500 mg/L), ciprofloxacin (200 mg/L), imipenem (250 mg/L) and metronidazole (1 g/L) in the drinking water. The intestinal colonization status of the mice was controlled once a week by highly sensitive cultural analysis of faecal samples. As early as 3 weeks after the start of broad-spectrum antibiotic treatment, quality controls indicated complete eradication of the intestinal microbiota, validated by negative results from both culture and molecular detection of bacteria using real-time PCR targeting the bacterial 16S rRNA genes. The mice were continuously kept in a sterile environment (autoclaved food and drinking water, sterile filtered antibiotic cocktail) and handled under strict aseptic conditions to

avoid contamination.

Lipoprotein separation and metabolite profiling

Plasma samples were subjected to fast-performance liquid chromatography (gel filtration on Superose 6 column (GE Healthcare)). Different lipoprotein fractions were separated and evaluated based on flow-through time. Cholesterol levels were quantified using an enzymatic assay (Cobas, Roche) according to the manufacturer's protocol. For metabolite profiling, mouse plasma samples (SCD n=4, HFD n=4 and HFD+PA n=4) were analyzed using a targeted metabolomics kit (MxP® Quant 500 kit: BIOCRATES Life Sciences AG, Innsbruck, Austria). For analysis of different lipid classes, a combination of liquid chromatography (Agilent 1290 Infinity II LC, Santa Clara, CA, USA) and mass spectrometry (AB SCIEX 5500 QTrap™ mass spectrometer; AB SCIEX, Darmstadt, Germany) was used. After normalization and pre-processing of the data, MetIDQ™ software (Biocrates) was used for peak integration and calculation of metabolite concentrations. Distinct cholesteryl esters were employed for further investigation in the present study.

Histology

Following sacrifice, basal segments of the mouse heart were immediately embedded in tissue-freezing medium (Leica) and frozen on dry ice. The tissues were stored at -80°C until further use. Sections of the aortic root (5 µm) were prepared on glass slides (Thermo Scientific, Super frost PLUS) using a Cryostat Microtome (Microm HM 560). Small intestinal tissues were fixed in paraffin. Sections (1-2 µm) were then stained with a polyclonal rabbit antibody (Novus Biologicals, #NB400-127) for detection of NPC1L1 protein. Images were analyzed and quantified with ImageJ Software.

Quantitative polymerase chain reaction

For quantitative polymerase chain reaction (qPCR), total RNA from the liver and ileum was isolated with TRIzol reagent (Invitrogen™; 15596026) following the manufacturer's instructions and quantified using absorbance measurements on a NanoDrop (Thermo Scientific™; ND-2000). Enzymatic DNA digestion was performed on total RNA from both tissues using RNase-free DNase I (1 U/µg; Thermo Scientific™; EN0251). Total RNA (1.0 µg) was used for the reverse transcription of hepatic RNA using the High-Capacity cDNA Reverse Transcription Kit (Applied Biosystems™; 4368814), and 0.7 µg of total RNA was used for the reverse transcription of RNA from intestinal tissue using the High-Capacity RNA-to-cDNA Kit (Applied Biosystems™; 4388950).

For intestinal organoids, cDNA synthesis and pre-amplification were performed using the SMART-PCR approach⁴⁵. In brief, 100ng of total RNA was mixed with 1 mM dNTPs (Thermo Fisher) and 10 µM of oligo-dT primer (5'-AAGCAGTGGTATCAACGCAGAGTACT30VN-3',

where “N” is any base and “V” is either “A,” “C” or “G”; Biomers), denatured and placed on ice. Then, the first-strand synthesis for each sample was achieved using 5 U/μl Maxima H minus reverse transcriptase (200 U/μl, Invitrogen), 1 U/μl Recombinant RNasin Ribonuclease Inhibitor (PROMEGA), 1x SuperScript VI Reverse Transcriptase (5x, Thermo fisher), 1 M betaine (5 M, Sigma), 10 mM MgCl²⁺ (1 mM, Thermo fisher), 1 μM ISPCR-TSO (Template Switching Oligos): 5'-AAGCAGTGGTATCAACGCAGAGTACATrGrG+G-3'; two riboguanosines (rG) and one LNA-modified guanosine (+G), and nuclease-free water (Invitrogen). Subsequently, the reverse transcriptase was inactivated, and an adapter – based PCR pre-amplification was carried out using 1x KAPA HiFi HotStart ReadyMix (2x, KAPA ROCHE), 200 nM ISPCR primers (10 μM, 5'AAGCAGTGGTATCAACGCAGAGT-3', Biomers) and nuclease-free water (Invitrogen). Finally, cDNA was treated with Exonuclease I (NEB) following the manufacturer's instructions.

Relative mRNA expression of hepatic genes (*Cyp7a1*, *Fxr*, *Hmgcr*, *Ldlr*, *Srebp2*, *Pcsk9*), intestinal genes (*Abca1*, *Abcg5*, *Acat2*, *Asbt*, *Npc111* and *Srb1*) and the reference gene *Gapdh* was analyzed using TaqMan Gene Expression Assays with the following primers (Applied Biosystems™; 4351372):

Gene	Species	Assay-ID
<i>Abca1</i>	Mouse	Mm00442646_m1
<i>Abcg5</i>	Mouse	Mm00446241_m1
<i>Acat2</i>	Mouse	Mm00782408_s1
<i>Asbt</i>	Mouse	Mm00488258_m1
<i>Cyp7a1</i>	Mouse	Mm00484150_m1
<i>Fxr</i>	Mouse	Mm00436425_m1
<i>Hmgcr</i>	Mouse	Mm01282499_m1
<i>Gapdh</i>	Mouse	Mm99999915_g1
<i>Ldlr</i>	Mouse	Mm01177349_m1
<i>Npc111</i>	Mouse	Mm01191973_m1
<i>Pcsk9</i>	Mouse	Mm01263610_m1
<i>Srb1</i>	Mouse	Mm00450234_m1
<i>Srebp2</i>	Mouse	Mm01306292_m1

Relative expression (triple determination) was examined by TaqMan Gene Expression Master Mix (Applied Biosystems™; 4369542) following the manufacturer's instructions.

RT-PCR

Reverse transcription-polymerase chain reaction (RT-PCR) was used to detect the expression of IL-10 receptor 1 (IL-10R1) in small intestinal organoids. The following gene-specific primer pairs for mouse IL10-R1 and IL10-R2 were manufactured by TIB Molbiol (TIB MOLBIOL Syntheselabor GmbH): IL10-R1: sense 5` AGG CAG AGG CAG CAG GCC CAG CAG AAT GCT 3`, antisense 5` TGG AGC CTG GCT AGC TGG TCA CAG TAG GTC 3`; IL10-R2: sense, 5` GCC AGC TCT AGG AAT GAT TC 3`, antisense 5` AAT GTT CTT CAA GGT CCA C 3`⁴⁶.

The mixture for each reaction was composed of primers (sense and antisense, 10 μ M each), BD (Rapidozym; GEN-OPTI-500), $MgCl^{2+}$ (25 mM; Rapidozym; GEN-OPTI-500), dNTPs (10 μ M; Rapidozym; GEN-009-250), and Taq polymerase (5 U/ μ l; Rapidozym; GEN-OPTI-500) following the manufacturer's instructions. cDNA (2 μ l) and RNase-free water were added to reach a volume of 20 μ l per well. PCR was performed with an initial denaturation at 95°C for 2 min, followed by 40 cycles of denaturation at 95°C for 30 s, annealing at 64°C for 30 s and extension at 72°C for 1 min. After complete amplification, DNA loading buffer (TaKaRaTM; 639285) was added, and the PCR products were visualized by electrophoresis on a 1.5% agarose gel (Agarose; ServaTM; 11406.02) (including 20 μ l of ethidium bromide and 90 ml of 1x Tris-acetate-EDTA-buffer). PeqGOLD DNA Ladder Mix (VWR Life ScienceTM; 25-2040) served as a molecular weight reference band following the manufacturer's instructions.

Statistical analyses

Database management and statistical analyses were performed with PRISM version 8.2.0 (GraphPad Software Inc., USA), IBM SPSS Statistics 25 (IBM, USA) and R⁴⁷ just as additional R packages⁴⁸.

Experimental study

Grubbs' test was performed to identify and exclude outliers. Continuous data were subjected to the Kolmogorov–Smirnov test and Shapiro–Wilk test to determine normality and were expressed as the mean \pm standard deviation (SD). A comparison of 2 groups was performed by a two-tailed unpaired t test and Mann-Whitney U test, as appropriate. To compare >2 groups, 1-way ANOVA followed by post hoc Tukey's test was performed. Significance was assumed at a two-sided *p < 0.05, **p < 0.01, or ***p < 0.001.

Human study

Treatment groups were compared based on analyses of covariance (ANCOVA), with difference between measurement at T2 and T0 as the dependent variable, adjusting for measurement at T0. For safety endpoints, we calculated univariate logistic regression models. A two-sided significance level of 5% was applied for all analyses. As we did not correct for multiple testing for secondary endpoints, p-values for secondary endpoints have to be interpreted as exploratory analyses. The primary approach to handle missing values was multiple imputation for all endpoints with less than 40% missing values. As a sensitivity analysis, we also performed a multiple imputation by treatment group for the primary endpoint, and complete-case analyses for all endpoints.

Gut microbiota

The statistical analyses and graphical representations of the microbiota were performed using R v.3.5.1⁴⁷ with packages phyloseq v.1.26⁴⁹ and ggplot2 v.3. The compositional dissimilarity of the dataset was investigated using the Bray-Curtis dissimilarity metric calculated on proportion-normalized data using the vegdist function from the vegan package. Principal Coordinate Analysis (PCoA) plots were created using the made4 and ggplot2 packages. Permutational MANOVA statistical tests on the Bray-Curtis dissimilarity were performed using the adonis function from the vegan package with 1000 permutations; significance was assumed for $p < 0.05$. Changes in community diversity were investigated using Shannon Diversity metrics using the estimate_richness function in the phyloseq package.

References

1. N. Townsend, L. Wilson, P. Bhatnagar, K. Wickramasinghe, M. Rayner, M. Nichols, Cardiovascular disease in Europe: Epidemiological update 2016*Eur. Heart J.* (2016), doi:10.1093/eurheartj/ehw334.
2. F. Mach, C. Baigent, A. L. Catapano, K. C. Koskinas, M. Casula, L. Badimon, M. J. Chapman, G. G. De Backer, V. Delgado, B. A. Ference, I. M. Graham, A. Halliday, U. Landmesser, B. Mihaylova, T. R. Pedersen, G. Riccardi, D. J. Richter, M. S. Sabatine, M. R. Taskinen, L. Tokgozoglou, O. Wiklund, 2019 ESC/EAS Guidelines for the management of dyslipidaemias: lipid modification to reduce cardiovascular risk, *Eur. Heart J.* (2020), doi:10.1093/eurheartj/ehz455.
3. F. J. Brunner, C. Waldeyer, F. Ojeda, V. Salomaa, F. Kee, S. Sans, B. Thorand, S. Giampaoli, P. Brambilla, H. Tunstall-Pedoe, M. Moitry, L. Iacoviello, G. Veronesi, G. Grassi, E. B. Mathiesen, S. Söderberg, A. Linneberg, H. Brenner, P. Amouyel, J. Ferrières, A. Tamosiunas, Y. P. Nikitin, W. Drygas, O. Melander, K. H. Jöckel, D. M. Leistner, J. E. Shaw, D. B. Panagiotakos, L. A. Simons, M. Kavousi, R. S. Vasan, R. P. F. Dullaart, S. G. Wannamethee, U. Risérus, S. Shea, J. A. de Lemos, T. Omland, K. Kuulasmaa, U. Landmesser, S. Blankenberg, T. Zeller, J. Kontto, S. Männistö, A. Metspalu, K. Lackner, P. Wild, A. Peters, C. Meisinger, C. Donfrancesco, S. G. Signorini, M. Alver, M. Woodward, F. Gianfagna, S. Costanzo, T. Wilsgaard, M. Eliasson, T. Jørgensen, H. Völzke, M. Dörr, M. Nauck, B. Schöttker, T. Lorenz, N. Makarova, R. Twerenbold, J. Dallongeville, A. Dobson, S. Malyutina, A. Pajak, G. Engström, M. Bobak, B. Schmidt, T. Jääskeläinen, T. Niiranen, P. Jousilahti, G. Giles, A. Hodge, J. Klotsche, D. J. Magliano, M. N. Lyngbakken, K. Hveem, C. Pitsavos, E. J. Benjamin, S. J. L. Bakker, P. Whincup, M. K. Ikram, M. Ingelsson, W. Koenig, Application of non-HDL cholesterol for population-based cardiovascular risk stratification: results from the Multinational Cardiovascular Risk Consortium, *Lancet* (2019), doi:10.1016/S0140-6736(19)32519-X.
4. V. R. Velagapudi, R. Hezaveh, C. S. Reigstad, P. Gopalacharyulu, L. Yetukuri, S. Islam, J. Felin, R. Perkins, J. Borén, M. Orešič, F. Bäckhed, The gut microbiota modulates host energy and lipid metabolism in mice, *J. Lipid Res.* (2010), doi:10.1194/jlr.M002774.
5. Z. Wang, A. B. Roberts, J. A. Buffa, B. S. Levison, W. Zhu, E. Org, X. Gu, Y. Huang, M. Zamanian-Daryoush, M. K. Culley, A. J. DiDonato, X. Fu, J. E. Hazen, D. Krajcik, J. A. DiDonato, A. J. Lusis, S. L. Hazen, Non-lethal Inhibition of Gut Microbial Trimethylamine Production for the Treatment of Atherosclerosis., *Cell* (2015), doi:10.1016/j.cell.2015.11.055.
6. R. A. Koeth, Z. Wang, B. S. Levison, J. A. Buffa, E. Org, B. T. Sheehy, E. B. Britt, X. Fu, Y. Wu, L. Li, J. D. Smith, J. A. DiDonato, J. Chen, H. Li, G. D. Wu, J. D. Lewis, M. Warriar, J. M. Brown, R. M. Krauss, W. H. W. Tang, F. D. Bushman, A. J. Lusis, S. L. Hazen, Intestinal microbiota metabolism of l-carnitine, a nutrient in red meat, promotes atherosclerosis, *Nat. Med.* (2013), doi:10.1038/nm.3145.
7. A. L. Jonsson, R. Caesar, R. Akrami, C. Reinhardt, F. F. Hållenius, J. Borén, F. Bäckhed, Impact of gut microbiota and diet on the development of atherosclerosis in ApoE^{-/-} mice, *Arterioscler. Thromb. Vasc. Biol.* (2018), doi:10.1161/ATVBAHA.118.311233.
8. K. Kasahara, K. A. Krautkramer, E. Org, K. A. Romano, R. L. Kerby, E. I. Vivas, M. Mehrabian, J. M. Denu, F. Bäckhed, A. J. Lusis, F. E. Rey, Interactions between *Roseburia intestinalis* and diet modulate atherogenesis in a murine model, *Nat. Microbiol.* (2018), doi:10.1038/s41564-018-0272-x.
9. E. Brandsma, N. J. Kloosterhuis, M. Koster, D. C. Dekker, M. J. J. Gijbels, S. Van Der Velden, M. Ríos-Morales, M. J. R. Van Faassen, M. G. Loreti, A. De Bruin, J. Fu, F. Kuipers, B. M. Bakker, M. Westerterp, M. P. J. De Winther, M. H. Hofker, B. Van De Sluis, D. P. Y. Koonen, A Proinflammatory Gut Microbiota Increases Systemic Inflammation and Accelerates Atherosclerosis, *Circ. Res.* (2019), doi:10.1161/CIRCRESAHA.118.313234.
10. N. Natarajan, D. Hori, S. Flavahan, J. Steppan, N. A. Flavahan, D. E. Berkowitz, J. L. Pluznick, Microbial short chain fatty acid metabolites lower blood pressure via endothelial G protein-coupled receptor 41, *Physiol. Genomics* (2016), doi:10.1152/physiolgenomics.00089.2016.
11. I. Nemet, P. P. Saha, N. Gupta, W. Zhu, K. A. Romano, S. M. Skye, T. Cajka, M. L. Mohan, L. Li, Y. Wu, M. Funabashi, A. E. Ramer-Tait, S. V. Naga Prasad, O. Fiehn, F. E. Rey, W. H. W. Tang, M. A. Fischbach, J. A. DiDonato, S. L. Hazen, A Cardiovascular Disease-Linked Gut Microbial Metabolite Acts

via Adrenergic Receptors, *Cell* (2020), doi:10.1016/j.cell.2020.02.016.

12. Z. Wang, E. Klipfell, B. J. Bennett, R. Koeth, B. S. Levison, B. DuGar, A. E. Feldstein, E. B. Britt, X. Fu, Y.-M. Chung, Y. Wu, P. Schauer, J. D. Smith, H. Allayee, W. H. W. Tang, J. A. DiDonato, A. J. Lusis, S. L. Hazen, Gut flora metabolism of phosphatidylcholine promotes cardiovascular disease, *Nature* **472**, 57–63 (2011).

13. W. H. W. Tang, Z. Wang, B. S. Levison, R. A. Koeth, E. B. Britt, X. Fu, Y. Wu, S. L. Hazen, Intestinal microbial metabolism of phosphatidylcholine and cardiovascular risk, *N. Engl. J. Med.* (2013), doi:10.1056/NEJMoa1109400.

14. W. H. W. Tang, Z. Wang, D. J. Kennedy, Y. Wu, J. A. Buffa, B. Agatista-Boyle, X. S. Li, B. S. Levison, S. L. Hazen, Gut microbiota-dependent trimethylamine N-oxide (TMAO) pathway contributes to both development of renal insufficiency and mortality risk in chronic kidney disease, *Circ. Res.* (2014), doi:10.1161/CIRCRESAHA.116.305360.

15. A. Haghikia, X. S. Li, T. G. Liman, N. Bledau, D. Schmidt, F. Zimmermann, N. Kränkel, C. Widera, K. Sonnenschein, A. Haghikia, K. Weissenborn, D. Fraccarollo, M. M. Heimesaat, J. Bauersachs, Z. Wang, W. Zhu, U. Bavendiek, S. L. Hazen, M. Endres, U. Landmesser, Gut microbiota-dependent trimethylamine N-oxide predicts risk of cardiovascular events in patients with stroke and is related to proinflammatory monocytes, *Arterioscler. Thromb. Vasc. Biol.* (2018), doi:10.1161/ATVBAHA.118.311023.

16. G. G. Schiattarella, A. Sannino, E. Toscano, G. Giugliano, G. Gargiulo, A. Franzone, B. Trimarco, G. Esposito, C. Perrino, Gut microbe-generated metabolite trimethylamine-N-oxide as cardiovascular risk biomarker: A systematic review and dose-response meta-analysis, *Eur. Heart J.* (2017), doi:10.1093/eurheartj/ehx342.

17. A. Koh, F. De Vadder, P. Kovatcheva-Datchary, F. Bäckhed, From dietary fiber to host physiology: Short-chain fatty acids as key bacterial metabolites *Cell* (2016), doi:10.1016/j.cell.2016.05.041.

18. D. M. Kaye, W. Shihata, H. A. Jama, K. Tsyganov, M. Ziemann, H. Kiriazis, D. Horlock, A. Vijay, B. Giam, A. Vinh, C. Johnson, A. Fiedler, D. Donner, M. Snelson, M. T. Coughlan, S. Phillips, X.-J. Du, A. El-Osta, G. Drummond, G. W. Lambert, T. Spector, A. M. Valdes, C. R. Mackay, F. Z. Marques, Deficiency of Prebiotic Fibre and Insufficient Signalling Through Gut Metabolite Sensing Receptors Leads to Cardiovascular Disease, *Circulation* (2020), doi:10.1161/circulationaha.119.043081.

19. P. M. Smith, M. R. Howitt, N. Panikov, M. Michaud, C. A. Gallini, M. Bohlooly-Y, J. N. Glickman, W. S. Garrett, The microbial metabolites, short-chain fatty acids, regulate colonic T reg cell homeostasis, *Science* (80-.). (2013), doi:10.1126/science.1241165.

20. A. Haghikia, S. Jörg, A. Duscha, J. Berg, A. Manzel, A. Waschbisch, A. Hammer, D. H. Lee, C. May, N. Wilck, A. Balogh, A. I. Ostermann, N. H. Schebb, D. A. Akkad, D. A. Grohme, M. Kleinewietfeld, S. Kempa, J. Thöne, S. Demir, D. N. Müller, R. Gold, R. A. Linker, Dietary Fatty Acids Directly Impact Central Nervous System Autoimmunity via the Small Intestine, *Immunity* (2015), doi:10.1016/j.immuni.2015.09.007.

21. A. Duscha, B. Gisevius, S. Hirschberg, R. A. Linker, R. Gold, A. Haghikia, Propionic Acid Shapes the Multiple Sclerosis Disease Course by an Immunomodulatory Mechanism, *Cell* (2020), doi:10.1016/j.cell.2020.02.035.

22. H. Bartolomeaus, A. Balogh, M. Yakoub, S. Homann, L. Markó, S. Höges, D. Tsvetkov, A. Krannich, S. Wundersitz, E. G. Avery, N. Haase, K. Kräker, L. Hering, M. Maase, K. Kusche-Vihrog, M. Grandoch, J. Fielitz, S. Kempa, M. Gollasch, Z. Zhumadilov, S. Kozhakhmetov, A. Kushugulova, K. U. Eckardt, R. Dechend, L. C. Rump, S. K. Forslund, D. N. Müller, J. Stegbauer, N. Wilck, Short-Chain Fatty Acid Propionate Protects from Hypertensive Cardiovascular Damage, *Circulation* (2019), doi:10.1161/CIRCULATIONAHA.118.036652.

23. F. L. Crowe, T. J. Key, P. N. Appleby, K. Overvad, E. B. Schmidt, R. Egeberg, A. Tjønneland, R. Kaaks, B. Teucher, H. Boeing, C. Weikert, A. Trichopoulou, V. Ouranos, E. Valanou, G. Masala, S. Sieri, S. Panico, R. Tumino, G. Matullo, H. B. Bueno-De-Mesquita, J. M. A. Boer, J. W. J. Beulens, Y. T. Van Der Schouw, J. R. Quirós, G. Buckland, M. J. Sánchez, M. Dorronsoro, J. M. Huerta, C. Moreno-Iribas, B. Hedblad, J. H. Jansson, P. Wennberg, K. T. Khaw, N. Wareham, P. Ferrari, A. K. Illner, S. C. Chuang,

- T. Norat, J. Danesh, E. Riboli, Dietary fibre intake and ischaemic heart disease mortality: The European Prospective Investigation into Cancer and Nutrition-Heart study, *Eur. J. Clin. Nutr.* (2012), doi:10.1038/ejcn.2012.51.
24. R. Klingenberg, N. Gerdes, R. M. Badeau, A. Gisterå, D. Strodthoff, D. F. J. Ketelhuth, A. M. Lundberg, M. Rudling, S. K. Nilsson, G. Olivecrona, S. Zoller, C. Lohmann, T. F. Lüscher, M. Jauhiainen, T. Sparwasser, G. K. Hansson, Depletion of FOXP3+ regulatory T cells promotes hypercholesterolemia and atherosclerosis, *J. Clin. Invest.* (2013), doi:10.1172/JCI63891.
25. E. D. Michos, J. W. McEvoy, R. S. Blumenthal, Lipid management for the prevention of atherosclerotic cardiovascular disease *N. Engl. J. Med.* (2019), doi:10.1056/NEJMra1806939.
26. S. W. Altmann, H. R. Davis, L. J. Zhu, X. Yao, L. M. Hoos, G. Tetzloff, S. P. N. Iyer, M. Maguire, A. Golovko, M. Zeng, L. Wang, N. Murgolo, M. P. Graziano, Niemann-Pick C1 Like 1 Protein Is Critical for Intestinal Cholesterol Absorption, *Science* (80-.). (2004), doi:10.1126/science.1093131.
27. P. A. Dawson, J. Haywood, A. L. Craddock, M. Wilson, M. Tietjen, K. Kluckman, N. Maeda, J. S. Parks, Targeted Deletion of the Ileal Bile Acid Transporter Eliminates Enterohepatic Cycling of Bile Acids in Mice, *J. Biol. Chem.* (2003), doi:10.1074/jbc.M306370200.
28. G. Silbernagel, G. Fauler, B. Genser, C. Drechsler, V. Krane, H. Scharnagl, T. B. Grammer, I. Baumgartner, E. Ritz, C. Wanner, W. März, Intestinal cholesterol absorption, treatment with atorvastatin, and cardiovascular risk in hemodialysis patients, *J. Am. Coll. Cardiol.* (2015), doi:10.1016/j.jacc.2015.03.551.
29. M. Huch, B. K. Koo, Modeling mouse and human development using organoid cultures *Dev.* (2015), doi:10.1242/dev.118570.
30. N. Arpaia, C. Campbell, X. Fan, S. Dikiy, J. Van Der Veeken, P. Deroos, H. Liu, J. R. Cross, K. Pfeffer, P. J. Coffey, A. Y. Rudensky, Metabolites produced by commensal bacteria promote peripheral regulatory T-cell generation, *Nature* (2013), doi:10.1038/nature12726.
31. S. He, F. Kahles, S. Rattik, M. Nairz, C. S. McAlpine, A. Anzai, D. Selgrade, A. M. Fenn, C. T. Chan, J. E. Mindur, C. Valet, W. C. Poller, L. Halle, N. Rotllan, Y. Iwamoto, G. R. Wojtkiewicz, R. Weissleder, P. Libby, C. Fernández-Hernando, D. J. Drucker, M. Nahrendorf, F. K. Swirski, Gut intraepithelial T cells calibrate metabolism and accelerate cardiovascular disease, *Nature* (2019), doi:10.1038/s41586-018-0849-9.
32. M. Biton, A. L. Haber, N. Rogel, G. Burgin, S. Beyaz, A. Schnell, O. Ashenberg, C. W. Su, C. Smillie, K. Shekhar, Z. Chen, C. Wu, J. Ordovas-Montanes, D. Alvarez, R. H. Herbst, M. Zhang, I. Tirosh, D. Dionne, L. T. Nguyen, M. E. Xifaras, A. K. Shalek, U. H. von Andrian, D. B. Graham, O. Rozenblatt-Rosen, H. N. Shi, V. Kuchroo, O. H. Yilmaz, A. Regev, R. J. Xavier, T Helper Cell Cytokines Modulate Intestinal Stem Cell Renewal and Differentiation, *Cell* (2018), doi:10.1016/j.cell.2018.10.008.
33. Wang J, Zhang H, Chen X, Chen Y, Menghebilige, Bao Q. Selection of potential probiotic lactobacilli for cholesterol-lowering properties and their effect on cholesterol metabolism in rats fed a high-lipid diet. *J Dairy Sci* 2012;doi: 10.3168/jds.2011-4768.
34. W. H. W. Tang, F. Bäckhed, U. Landmesser, S. L. Hazen, Intestinal Microbiota in Cardiovascular Health and Disease: JACC State-of-the-Art Review *J. Am. Coll. Cardiol.* (2019), doi:10.1016/j.jacc.2019.03.024.
35. G. S. Berenson, S. R. Srinivasan, W. Bao, W. P. Newman, R. E. Tracy, W. A. Wattigney, Association between multiple cardiovascular risk factors and atherosclerosis in children and young adults, *N. Engl. J. Med.* (1998), doi:10.1056/NEJM199806043382302.
36. K. K. Ray, U. Laufs, F. Cosentino, M. D. Lobo, U. Landmesser, The year in cardiology: Cardiovascular prevention, *Eur. Heart J.* (2020), doi:10.1093/eurheartj/ehz929.
37. B. A. Ference, H. N. Ginsberg, I. Graham, K. K. Ray, C. J. Packard, E. Bruckert, R. A. Hegele, R. M. Krauss, F. J. Raal, H. Schunkert, G. F. Watts, J. Borén, S. Fazio, J. D. Horton, L. Masana, S. J. Nicholls, B. G. Nordestgaard, B. van de Sluis, M.-R. Taskinen, L. Tokgözoğlu, U. Landmesser, U. Laufs,

- O. Wiklund, J. K. Stock, M. J. Chapman, A. L. Catapano, Low-density lipoproteins cause atherosclerotic cardiovascular disease. 1. Evidence from genetic, epidemiologic, and clinical studies. A consensus statement from the European Atherosclerosis Society Consensus Panel, *Eur. Heart J.* (2017), doi:10.1093/eurheartj/ehx144.
38. Z. Jie, H. Xia, S. L. Zhong, Q. Feng, S. Li, S. Liang, H. Zhong, Z. Liu, Y. Gao, H. Zhao, D. Zhang, Z. Su, Z. Fang, Z. Lan, J. Li, L. Xiao, J. Li, R. Li, X. Li, F. Li, H. Ren, Y. Huang, Y. Peng, G. Li, B. Wen, B. Dong, J. Y. Chen, Q. S. Geng, Z. W. Zhang, H. Yang, J. Wang, J. Wang, X. Zhang, L. Madsen, S. Brix, G. Ning, X. Xu, X. Liu, Y. Hou, H. Jia, K. He, K. Kristiansen, The gut microbiome in atherosclerotic cardiovascular disease, *Nat. Commun.* (2017), doi:10.1038/s41467-017-00900-1.
39. T. W. H. Tang, H. C. Chen, C. Y. Chen, C. Y. T. Yen, C. J. Lin, R. P. Prajnamitra, L. L. Chen, S. C. Ruan, J. H. Lin, P. J. Lin, H. H. Lu, C. W. Kuo, C. M. Chang, A. D. Hall, E. I. Vivas, J. W. Shui, P. Chen, T. A. Hacker, F. E. Rey, T. J. Kamp, P. C. H. Hsieh, Loss of Gut Microbiota Alters Immune System Composition and Cripples Postinfarction Cardiac Repair, *Circulation* (2019), doi:10.1161/CIRCULATIONAHA.118.035235.
40. A. B. Kimball, T. Kawamura, K. Tejura, C. Boss, A. R. Hancox, J. C. Vogel, S. M. Steinberg, M. L. Turner, A. Blauvelt, Clinical and immunologic assessment of patients with psoriasis in a randomized, double-blind, placebo-controlled trial using recombinant human interleukin 10, *Arch. Dermatol.* (2002), doi:10.1001/archderm.138.10.1341.
41. I. H. Chan, D. Van Hoof, M. Abramova, M. Bilardello, E. Mar, B. Jorgensen, S. McCauley, H. Bal, M. Oft, P. Van Vlasselaer, J. B. Mumm, Pegylated il-10 activates kupffer cells to control hypercholesterolemia *PLoS One* (2016), doi:10.1371/journal.pone.0156229.
42. A. Tirosh, E. S. Calay, G. Tuncman, K. C. Claiborn, K. E. Inouye, K. Eguchi, M. Alcalá, M. Rathaus, K. S. Hollander, I. Ron, R. Livne, Y. Heianza, L. Qi, I. Shai, R. Garg, G. S. Hotamisligil, The short-chain fatty acid propionate increases glucagon and FABP4 production, impairing insulin action in mice and humans, *Sci. Transl. Med.* (2019), doi:10.1126/scitranslmed.aav0120.
43. F. De Vadder, P. Kovatcheva-Datchary, D. Goncalves, J. Vinera, C. Zitoun, A. Duchamp, F. Bäckhed, G. Mithieux, Microbiota-generated metabolites promote metabolic benefits via gut-brain neural circuits, *Cell* (2014), doi:10.1016/j.cell.2013.12.016.
44. T. B. Shubitowski, B. G. Poll, N. Natarajan, J. L. Pluznick, Short-chain fatty acid delivery: assessing exogenous administration of the microbiome metabolite acetate in mice, *Physiol. Rep.* (2019), doi:10.14814/phy2.14005.
45. S. Picelli, Å. K. Björklund, O. R. Faridani, S. Sagasser, G. Winberg, R. Sandberg, Smart-seq2 for sensitive full-length transcriptome profiling in single cells, *Nat. Methods* (2013), doi:10.1038/nmeth.2639.
46. T. L. Denning, N. A. Campbell, F. Song, R. P. Garofalo, G. R. Klimpel, V. E. Reyes, P. B. Ernst, Expression of IL-10 receptors on epithelial cells from the murine small and large intestine, *Int. Immunol.* (2000), doi:10.1093/intimm/12.2.133.
47. T. Sato, R. G. Vries, H. J. Snippert, M. Van De Wetering, N. Barker, D. E. Stange, J. H. Van Es, A. Abo, P. Kujala, P. J. Peters, H. Clevers, Single Lgr5 stem cells build crypt-villus structures in vitro without a mesenchymal niche, *Nature* (2009), doi:10.1038/nature07935.
48. J. Lembcke, U. Ceglarek, G. M. Fiedler, S. Baumann, A. Leichtle, J. Thiery, Rapid quantification of free and esterified phytosterols in human serum using APPI-LC-MS/MS, *J. Lipid Res.* (2005), doi:10.1194/jlr.C400004-JLR200.
49. P. I. Costea, G. Zeller, S. Sunagawa, E. Pelletier, A. Alberti, F. Levenez, M. Tramontano, M. Driessen, R. Hercog, F. E. Jung, J. R. Kultima, M. R. Hayward, L. P. Coelho, E. Allen-Vercoe, L. Bertrand, M. Blaut, J. R. M. Brown, T. Carton, S. Cools-Portier, M. Daigneault, M. Derrien, A. Druesne, W. M. De Vos, B. B. Finlay, H. J. Flint, F. Guarner, M. Hattori, H. Heilig, R. A. Luna, J. Van Hylckama Vlieg, J. Junick, I. Klymiuk, P. Langella, E. Le Chatelier, V. Mai, C. Manichanh, J. C. Martin, C. Mery, H. Morita, P. W. O'toole, C. Orvain, K. R. Patil, J. Penders, S. Persson, N. Pons, M. Popova, A. Salonen, D. Saulnier, K. P. Scott, B. Singh, K. Slezak, P. Veiga, J. Versalovic, L. Zhao, E. G. Zoetendal, S. D.

- Ehrlich, J. Dore, P. Bork, Towards standards for human fecal sample processing in metagenomic studies, *Nat. Biotechnol.* (2017), doi:10.1038/nbt.3960.
50. M. Deschasaux, K. E. Bouter, A. Prodan, E. Levin, A. K. Groen, H. Herrema, V. Tremaroli, G. J. Bakker, I. Attaye, S. J. Pinto-Sietsma, D. H. van Raalte, M. B. Snijder, M. Nicolaou, R. Peters, A. H. Zwinderman, F. Bäckhed, M. Nieuwdorp, Depicting the composition of gut microbiota in a population with varied ethnic origins but shared geography, *Nat. Med.* (2018), doi:10.1038/s41591-018-0160-1.
51. R. C. Edgar, Search and clustering orders of magnitude faster than BLAST, *Bioinformatics* (2010), doi:10.1093/bioinformatics/btq461.
52. B. J. Callahan, P. J. McMurdie, S. P. Holmes, Exact sequence variants should replace operational taxonomic units in marker-gene data analysis, *ISME J.* (2017), doi:10.1038/ismej.2017.119.
53. R. C. Edgar, UNOISE2: improved error-correction for Illumina 16S and ITS amplicon sequencing, *bioRxiv* (2016), doi:10.1101/081257.
54. B. J. Callahan, P. J. McMurdie, M. J. Rosen, A. W. Han, A. J. A. Johnson, S. P. Holmes, DADA2: High-resolution sample inference from Illumina amplicon data, *Nat. Methods* (2016), doi:10.1038/nmeth.3869.
55. R. core Team, R: A Language and Environment for Statistical Computing, *R Found. Stat. Comput. Vienna, Austria* (2018).
56. H. Wickham, M. Averick, J. Bryan, W. Chang, L. McGowan, R. François, G. Grolemund, A. Hayes, L. Henry, J. Hester, M. Kuhn, T. Pedersen, E. Miller, S. Bache, K. Müller, J. Ooms, D. Robinson, D. Seidel, V. Spinu, K. Takahashi, D. Vaughan, C. Wilke, K. Woo, H. Yutani, Welcome to the Tidyverse, *J. Open Source Softw.* (2019), doi:10.21105/joss.01686.
57. P. J. McMurdie, S. Holmes, Phyloseq: An R Package for Reproducible Interactive Analysis and Graphics of Microbiome Census Data, *PLoS One* (2013), doi:10.1371/journal.pone.0061217.
58. J. Wang, H. Zhang, X. Chen, Y. Chen, Menghebilige, Q. Bao Q. Selection of potential probiotic lactobacilli for cholesterol-lowering properties and their effect on cholesterol metabolism in rats fed a high-lipid diet. *J Dairy Sci.* 2012 Apr;95(4):1645-54. doi: 10.3168/jds.2011-4768.

Figure Legends

Figure 1 The gut microbiota regulates cholesterol metabolism and impacts atherogenesis

(A - D) HPLC analysis of blood levels of total cholesterol, LDL cholesterol, VLDL cholesterol and HDL cholesterol in conventionally raised (Conv, black circles) or antibiotic treated (ABS, white circles) *ApoE*^{-/-} mice fed either a SCD or a HFD (Conv: SCD n=12, HFD n=10; ABS: SCD n=4, HFD n=7). (E and F) Representative HPLC-assisted fractionation of plasma lipids under a SCD or a HFD. (G and H) Representative images of Oil Red O-stained aortic root sections (scale bars represent 100 μ m) with quantification of lipid deposition (Conv, black circles: SCD n=8, HFD n=8; ABS, white circles: SCD n=5, HFD n=6). Data were analyzed by a two-tailed unpaired t test between two groups.

Figure 2 Propionate prevents HFD-induced hypercholesterolemia and atherosclerosis in *ApoE*^{-/-} mice

(A) *ApoE*^{-/-} mice were fed either a standard chow diet (SCD, n=12) or a high-fat diet (HFD, n=24) for 6 weeks. After 2 weeks, the SCD-fed mice received sodium chloride (vehicle), and the HFD-fed mice were treated with either propionate (PA, n=13) or sodium chloride (vehicle, n=11) via oral gavage until the end of the experiment. (B - E) HPLC analysis of blood levels of total cholesterol, LDL cholesterol, VLDL cholesterol and HDL cholesterol in *ApoE*^{-/-} mice at the end of the experiments (SCD n=12, HFD n=10, HFD + PA n=13). (F) Representative HPLC-assisted fractionation of plasma lipids. (G and H) Representative images of Oil Red O-stained aortic root sections (scale bars represent 100 μ m) with quantification of lipid deposition (SCD n=8, HFD n=8, HFD + PA n=11). For the analysis in B - H, the results of the Conv SCD and Conv HFD groups were the same results used in Figure 1. Data were analyzed by 1-way ANOVA followed by post hoc Tukey's test.

Figure 3 Effect of propionate on expression of genes involved in hepatic and intestinal cholesterol metabolism

(A - E) Expression of hepatic *Srebp2*, *Cyp7a1*, *Ldlr*, and small intestinal *Npc1l1* and *Asbt*, as assessed by qPCR at the end of the treatment (SCD n=11-12, HFD n=10-11 and HFD+PA

n=12-13). **(F)** Representative immunostaining (scale bars represent 100 μ m) of the small intestine of mice using an NPC1L1 antibody (upper row, immunohistochemistry; lower row, immunofluorescence) with **(G)** quantification of the mean fluorescence intensity (SCD n=9, HFD n=7 and HFD+PA n=9). **(H and I)** Analysis of blood levels of the phytosterols stigmasterol and sitosterol at the end of the experiments (SCD n=11, HFD n=10-11, HFD + PA n=13). Data were analyzed by 1-way ANOVA followed by post hoc Tukey's test.

Figure 4 Treatment with propionate increases Tregs and IL-10 in the small intestine

(A) Representative FACS plots of Tregs in the mesenteric lymph nodes (MLNs) from mice in the SCD, HFD and HFD+PA groups. **(B and C)** Compared to the SCD (n=7), the HFD (n=7) reduced Tregs in the MLNs and peripheral blood, and this change was reversed by PA treatment (n=7-8). **(D)** Tregs in the spleen were not altered by HFD or PA. **(E – I)** Cytokine analysis of the small intestine revealed an increase in IL-10 levels after treatment with PA, whereas the levels of TNF- α , MCP-1, IL-6 and INF- γ were not altered by PA. Data were analyzed by 1-way ANOVA followed by post hoc Tukey's test.

Figure 5 Regulation of *Npc111* gene expression by IL-10 mediates propionate-dependent control of intestinal cholesterol absorption and atheroprotection

(A) Representative photomicrograph of a mouse small intestinal epithelial organoid. **(B)** The organoids express both the IL-10R1 and IL-10R2 receptors, as demonstrated by RT-PCR. **(C)** Treatment of the organoids with murine recombinant IL-10 downregulated the expression of the *Npc111* gene in a dose-dependent manner (n=4 independent biological replicates). **(D)** IL-10 signaling was inhibited by weekly i.p. injection of a monoclonal blocking antibody against the IL-10 receptor in HFD-fed *Apoe*^{-/-} mice during the PA treatment period (HFD+PA n=13, HFD+PA+IL10R AB n=8). **(E - H)** HPLC analysis of blood levels of total cholesterol, LDL cholesterol, VLDL cholesterol and HDL cholesterol in HFD+PA mice in the presence (grey) or absence (blue) of IL-10R AB. **(I)** Representative HPLC-assisted fractionation of plasma lipids. **(J and K)** Representative images of Oil Red O-stained aortic root sections (scale bars represent 100 μ m) with quantification of lipid deposition (HFD+PA n=11, HFD+PA+IL10R AB n=7). **(L and M)** Analysis of blood levels of the phytosterols stigmasterol and sitosterol at the end of the experiments (HFD+PA n=13, HFD+PA+IL10R AB n=8). For the analysis in **E - M**, the results for the HFD+PA group were the same results used in Figure 2. Data were analyzed by a two-tailed unpaired t test.

Figure 6 Oral propionate supplementation lowers blood LDL and total cholesterol levels in hypercholesterolemic humans

(A and B) Waterfall plots depict the change in LDL and total cholesterol levels a from baseline to week 8 for each study participant randomly assigned to the placebo group and the PA group. **(C and D)** Box plots illustrate the distribution of LDL and total cholesterol levels within the placebo (red) and propionate (blue) groups for each timepoint (baseline and after 8 weeks). **(E and F)** Waterfall plots showing the change in non-HDL and HDL cholesterol levels. **(G and H)** Box plots demonstrating the distribution of non-HDL and HDL cholesterol levels for each timepoint. The lines depict the raw values at baseline and after 8 weeks. In the box plots, the line in the middle of the box indicates the median, and the lower and upper limits of the box correspond to the 25th and 75th percentiles, respectively. Analysis of covariance (ANCOVA, CI: confidence intervals) was performed to test the delta change between the two groups (placebo n=29, propionate n=29).

Figure 7 Effect of oral propionate supplementation on body weight

(A) Waterfall plots depict the change in body weight from baseline to week 8 for each study participant randomly assigned to the placebo group and the PA group. **(B)** Box plots illustrate the distribution of body weight within the placebo (red) and propionate (blue) groups for each timepoint (baseline and after 8 weeks). The lines depict the raw values at baseline and after 8 weeks. In the box plots, the line in the middle of the box indicates the median, and the lower and upper limits of the box correspond to the 25th and 75th percentiles, respectively. Analysis of covariance (ANCOVA, CI: confidence intervals) was performed to test the delta change between the two groups (placebo n=29, propionate n=29).

Suppl Figure S1

Graphs demonstrate that application of the vehicle (0.9% sodium chloride) per oral gavage did not alter levels of blood lipids irrespective of the diet (without vehicle n=10, white vehicle n =7). Data were analyzed by a two-tailed unpaired t test between two groups.

Suppl Figure S2 Exogenous propionate prevents HFD-induced increases in distinct cholesteryl esters

Blood levels of selected cholesteryl esters in *Apoe*^{-/-} mice fed a SCD (black circles, n=4), a HFD without propionate (red circles, n=3-4) or a HFD with propionate (PA, blue circles, n=3-4). Data were analyzed by 1-way ANOVA followed by post hoc Tukey's test. *p < 0.05, **p < 0.01, ***p < 0.001.

Suppl Figure S3 Effect of propionate on HFD-induced hypercholesterolemia and atherosclerosis in antibiotic treated *Apoe*^{-/-} mice

(A - D) HPLC analysis of blood levels of total cholesterol, LDL cholesterol, VLDL cholesterol and HDL cholesterol in antibiotic treated (ABS) *ApoE*^{-/-} mice fed a HFD without propionate (n=7) or with propionate (n=6). **(E)** Representative HPLC-assisted fractionation of plasma lipids. **(F and G)** Representative images of Oil Red O-stained aortic root sections (scale bars represent 100 μm) with quantification of lipid deposition (ABS+HFD: n=6, ABS+HFD+PA: n=6). The results of the ABS+HFD group were the same results used in Figure 1. Data were analyzed by a two-tailed unpaired t test between two groups.

Suppl Figure S4 Effect of propionate on the expression of hepatic genes involved in cholesterol metabolism and HMG-CoA reductase activity

(A – C) Expression of hepatic *Pcsk9*, *Hmgcr* and *Fxr*, as assessed by qPCR at the end of the treatment (SCD n=12, HFD n=11 and HFD+PA n=11-12). **D**, Analysis of the enzyme activity of HMG-CoA reductase with increasing concentrations of propionate and two concentrations of atorvastatin as a positive control (n=4). Data were analyzed by 1-way ANOVA followed by post hoc Tukey's test.

Suppl Figure S5 Effect of exogenous propionate on the expression of genes involved in transintestinal cholesterol absorption and efflux

A through C, Expression of small intestinal *Abcg5*, *Acat2* and *Abca1*, as assessed by qPCR at the end of the treatment (SCD n=11-12, HFD n=9-11 and HFD+PA n=12-13). Data were analyzed by 1-way ANOVA followed by post hoc Tukey's test.

Suppl Figure S6 Exogenous propionate increased fecal cholesterol level in HFD fed mice

Graph depicts fecal cholesterol levels in HFD fed mice after 4 weeks without (n=4) and with PA (n=4) treatment. Data were analyzed by a two-tailed unpaired t test between two groups.

Suppl Figure S7 *Npc1l1* gene expression in small intestinal organoids in response to propionate treatment

Treatment of murine small intestinal organoids with different concentrations of propionate did not affect the expression of the *Npc1l1* gene (n=4 independent biological replicates). Data were analyzed by 1-way ANOVA followed by post hoc Tukey's test.

Suppl Figure S8 Effect of propionate on Th1 and Th17 cell frequencies

A through C, The graphs in the upper row represent the cell frequencies of Th1 cells measured by flow cytometry in the MLNs, whole blood and spleen as percentages of CD4⁺ cells (SCD n=7-8, HFD n=6-9 and HFD+PA n=7-11). **D through F**, The graphs in the lower row represent

the cell frequencies of Th17 cells in the MLNs, whole blood and spleen as percentages of CD4⁺ cells (SCD n=6-7, HFD n=6-9 and HFD+PA n=6-10). Data were analyzed by 1-way ANOVA followed by post hoc Tukey's test.

Suppl Figure S9 Flow chart of the interventional study testing the effect of oral propionate in hypercholesterolemic humans

The diagram illustrates screening, randomization to either the placebo or propionate group, and follow-up of the participants, with the number of individuals at each step of the study progress.

Suppl Figure S10 Effect of oral propionate supplementation on plasma propionate levels and gut microbiota profiles

A, Box plots show the intra-individual change of the propionate concentration after 8 weeks within the placebo (red) and propionate groups (blue) in a subset of participants. Analysis of covariance (ANCOVA; CI: confidence intervals) was performed to test the delta change between the two groups (placebo n=21, propionate n=21). **B** and **C**, Gut microbiota analyses in a subset of participants (placebo n=17, propionate n=17) show no change either in β -diversity (Bray-Curtis dissimilarity, p=0.073 Adonis) or α -diversity (Shannon diversity index, p=0.357 ANOVA) within the placebo and propionate groups.

Suppl Figure S11 Effect of oral propionate supplementation on Treg levels in humans

A, Box plots illustrate the distribution of Treg levels (as percent of CD4⁺ cells) in the peripheral blood within the placebo (red) and propionate (blue) groups for each timepoint (baseline and after 8 weeks). **B**, Representative FACS plots of Tregs in the peripheral blood at baseline and after 8 weeks. Analysis of covariance (ANCOVA; CI: confidence intervals) was performed to test the delta change between the two groups (placebo n=29, propionate n=29).

Suppl Figure S12 Effect of oral propionate supplementation on T helper cell numbers in humans

A and **B**, Box plots illustrate the distribution of Th17 and Th1 levels (as a percentage of CD4⁺ cells) in the peripheral blood within the placebo (red) and propionate (blue) groups for each timepoint (baseline and after 8 weeks). Analysis of covariance (ANCOVA; CI: confidence intervals) was performed to test the delta change between the two groups (placebo n=29, propionate n=29).

Suppl Figure 13 Effect of oral propionate on plasma levels of fatty acid-binding protein 4 and glucagon

Box plots illustrate the distribution of plasma levels of **(A)** fatty acid-binding protein 4 and **(B)** glucagon within the placebo (red) and propionate (blue) groups for each timepoint (baseline and after 8 weeks). Analysis of covariance (ANCOVA, CI: confidence intervals) was performed to test the delta change between the two groups (placebo n=29, propionate n=29).

Graphical Model

The figure illustrates the proposed model of the cholesterol-lowering and atheroprotective properties of propionate. A high-fat high-cholesterol diet causes a disbalance of immune cells in the small intestinal microenvironment, with reduced Treg frequencies and IL-10 concentrations. Altered Treg levels are rescued upon exogenous propionate supplementation, with increased local levels. This in turn modulates NPC1L1 expression and membrane density, with a subsequent reduction in cholesterol absorption, ultimately leading to reduced atherogenesis. The illustration was adopted from Servier Medical Art (<http://smart.servier.com/>), licensed under a Creative Common Attribution 3.0 Generic License.

Acknowledgments

This study was supported by the Foundation Leducq network “Gut microbiome as a target for the treatment of cardiometabolic diseases”, Sympath (“Systems-medicine of pneumonia-aggravated atherosclerosis”, grant number 01ZX1906B) funded by the German Federal Ministry of Education and Research (BMBF), and by grants from the German Heart Research Foundation (DSHF F/28/16), German Center for Cardiovascular Research (DZHK, Rotation Grant), the Else Kröner-Fresenius-Stiftung (2017_A100), the German Research Foundation (DFG, HA 6951/2-1). Arash Haghikia is participant in the BIH-Charité Advanced Clinician Scientist Pilotprogram funded by the Charité – Universitätsmedizin Berlin and the Berlin Institute of Health. CMS, IN and SLH were also supported in part by grants from the National Institutes of Health and the Office of Dietary Supplements (P01HL147823, and R01HL103866). We thank Manuela Krämer for assistance in profiling the fecal microbiota. The computations microbiota analyses were performed on resources provided by SNIC through Uppsala Multidisciplinary Center for Advanced Computational Science (UPPMAX) under Project SNIC 2018-3-350. ANH is supported by a Lichtenberg fellowship by Volkswagen Foundation, a Berlin Institute of Health Clinician Scientist grant and German Research Foundation (DFG-TRR241-A05, INST 335/597-1). EPCvdV is supported by a grant from the Interdisciplinary Center for Clinical Research within the faculty of Medicine at the RWTH Aachen University, the DZHK (German Centre for Cardiovascular Research) and the BMBF (German Ministry of Education and Research), the Else Kröner Fresenius-Stiftung

(2018_A123) and NWO-ZonMw Veni (91619053). The anti-IL10R antibody (clone 1B1.2) was kindly provided by the DRFZ core facility.

Declaration of interests

SLH reports being named as co-inventor on pending and issued patents held by the Cleveland Clinic relating to cardiovascular diagnostics and therapeutics, being a paid consultant for P&G, having received research funds from P&G, and Roche Diagnostics, and being eligible to receive royalty payments for inventions or discoveries related to cardiovascular diagnostics or therapeutics from Cleveland HeartLab, Quest Diagnostics and P&G. The other authors have reported that they have no relationships relevant to the contents of this paper to disclose.

Contributions

Ar.H., D.N.M, R.G., Ai.H., F.B., S.L.H. and U.L. conceived the study. Ar.H., Ai.H., and U.L. supervised the study and wrote the manuscript with input from all authors. AiH and U.L. contributed equally as senior authors. Ar.H., F.H., A.J., J.R., D.S., J.K., V.N., C.R., A.N.H., E.P.C.v.d.V., V.D., N.K., M.M.H., S.B., O.S. and U.S. conducted experiments. P.S., P.H., and D.M.L performed the human study. G.R. and AA performed statistical analyses of the human study. U.C. performed LC-MS/MS. I.N., C.M.S., and S.L.H. performed GC-MS/MS. V.T., C.D., and F.B performed and analyzed 16S rRNA gene sequencing of faecal microbiota.

Figure 1

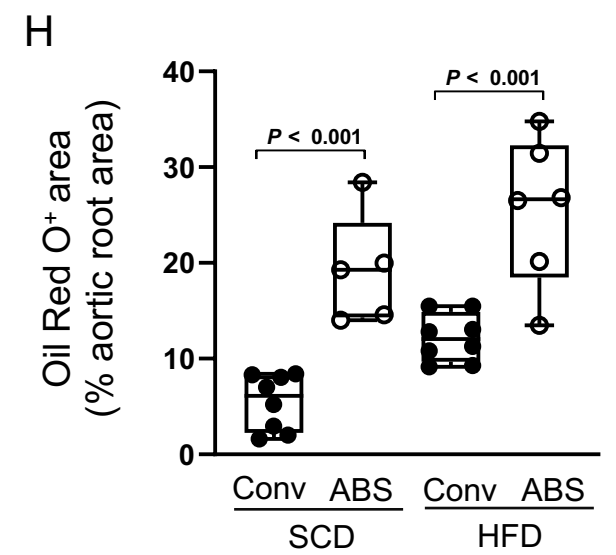
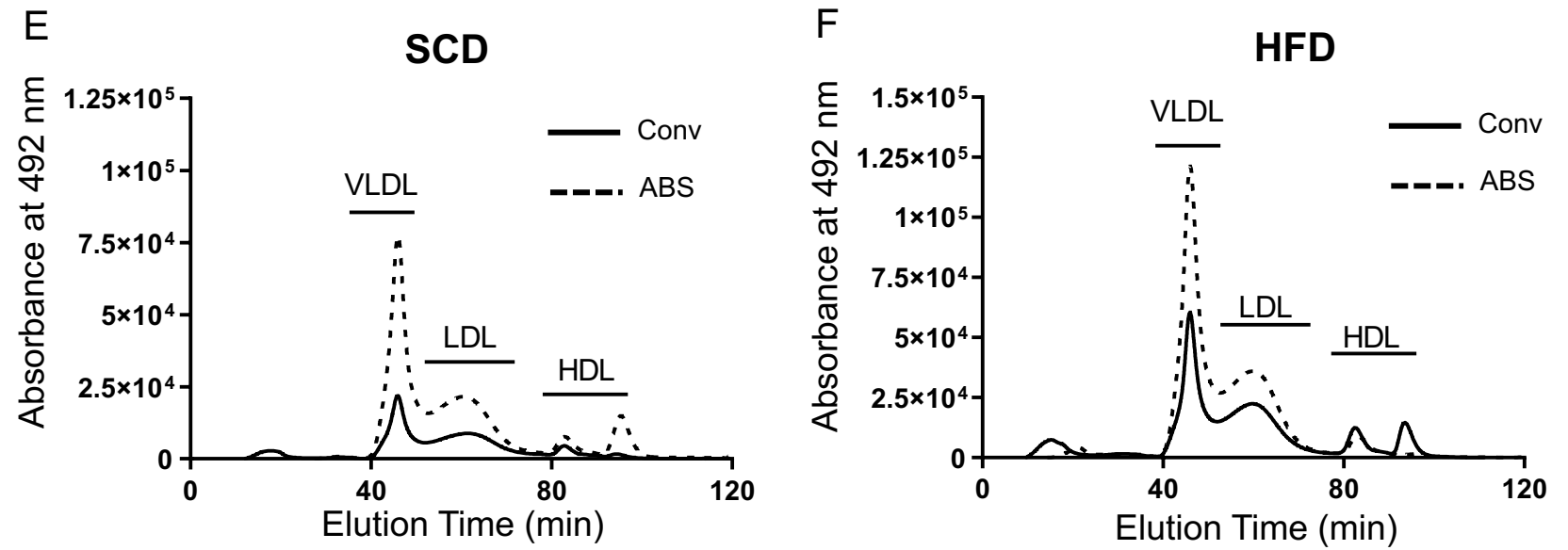
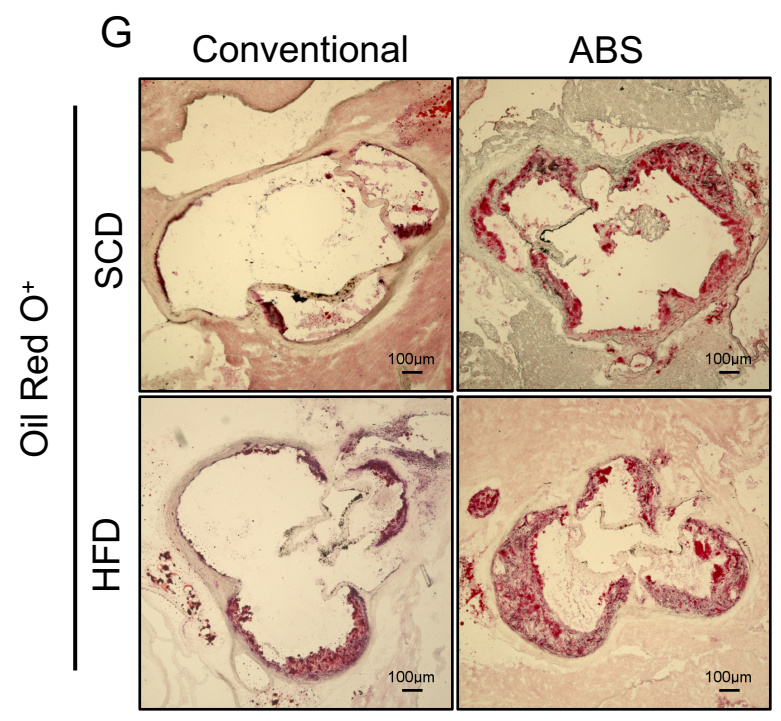
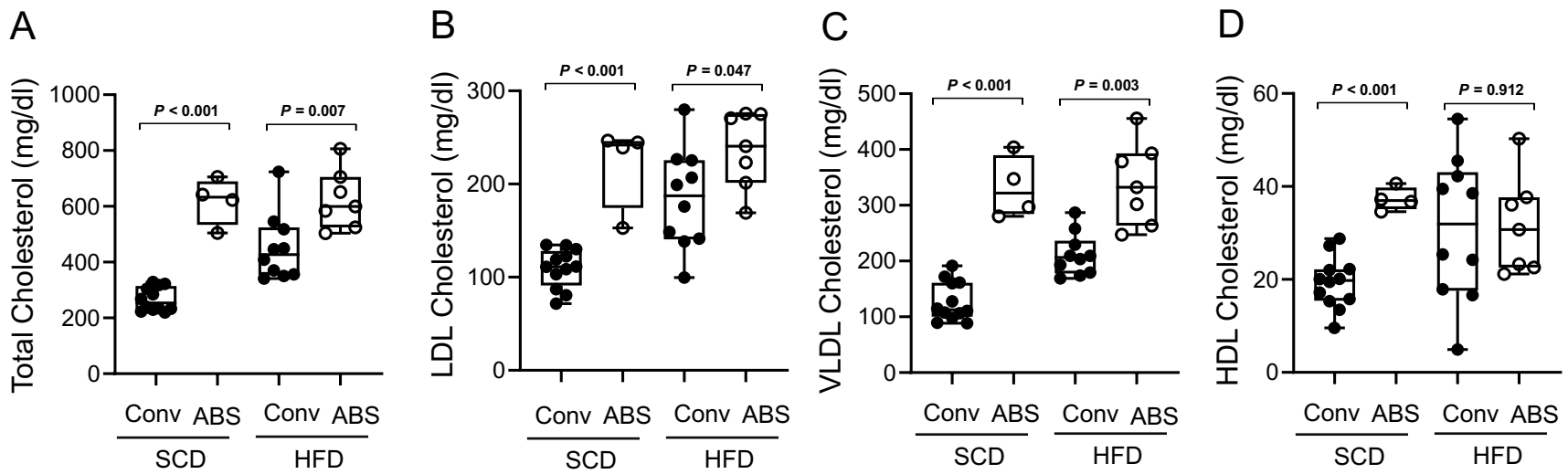


Figure 2

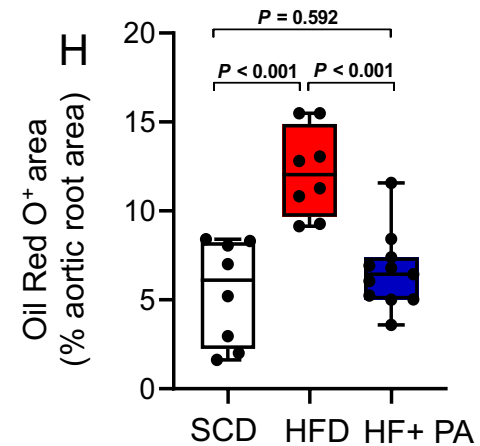
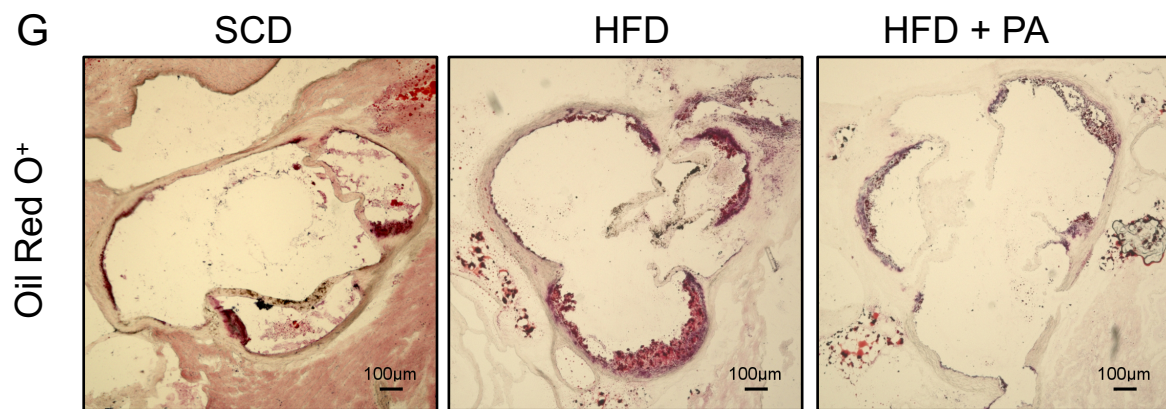
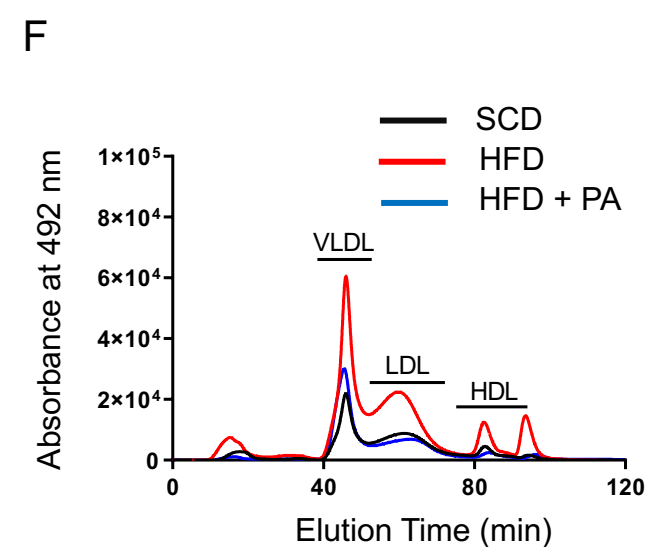
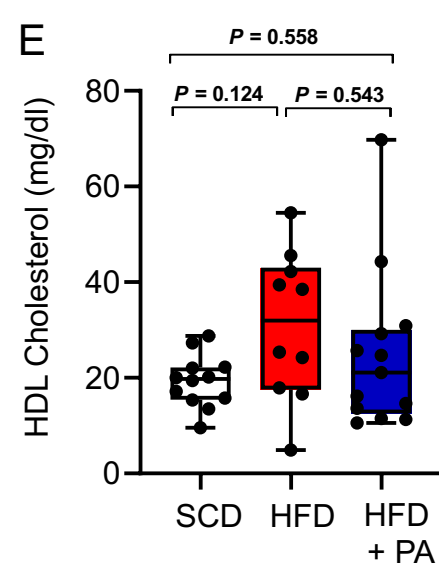
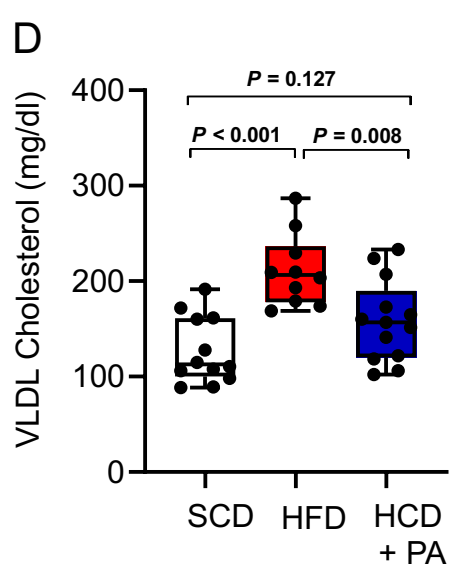
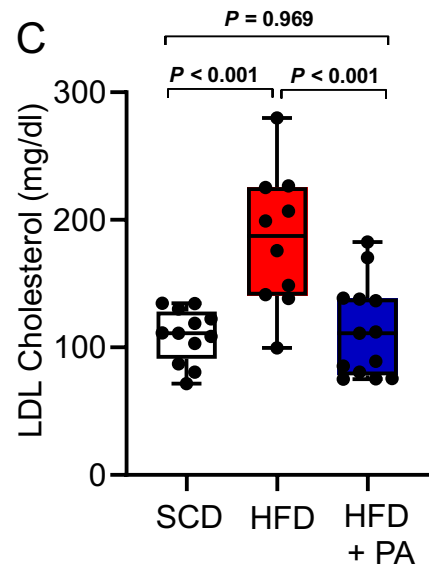
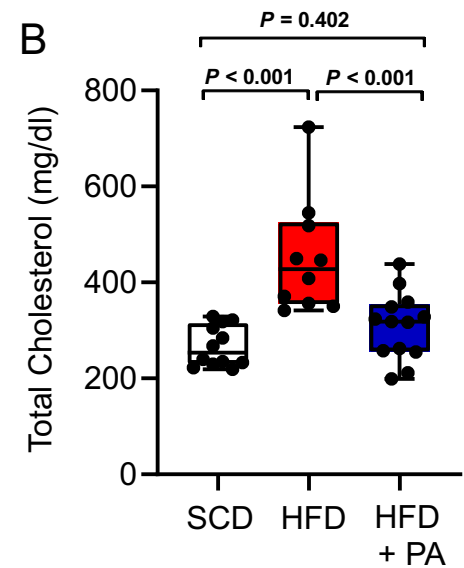
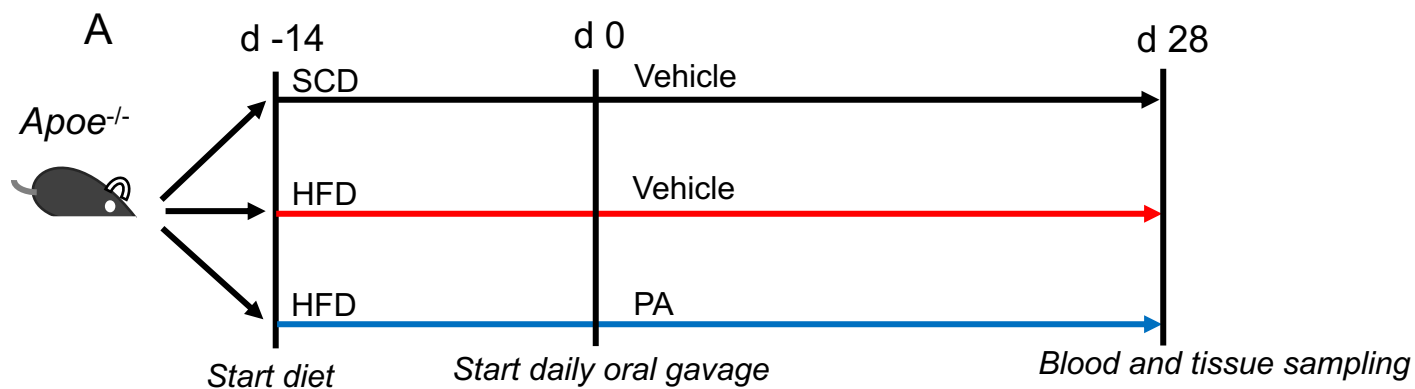


Figure 3

Liver

Small Intestine

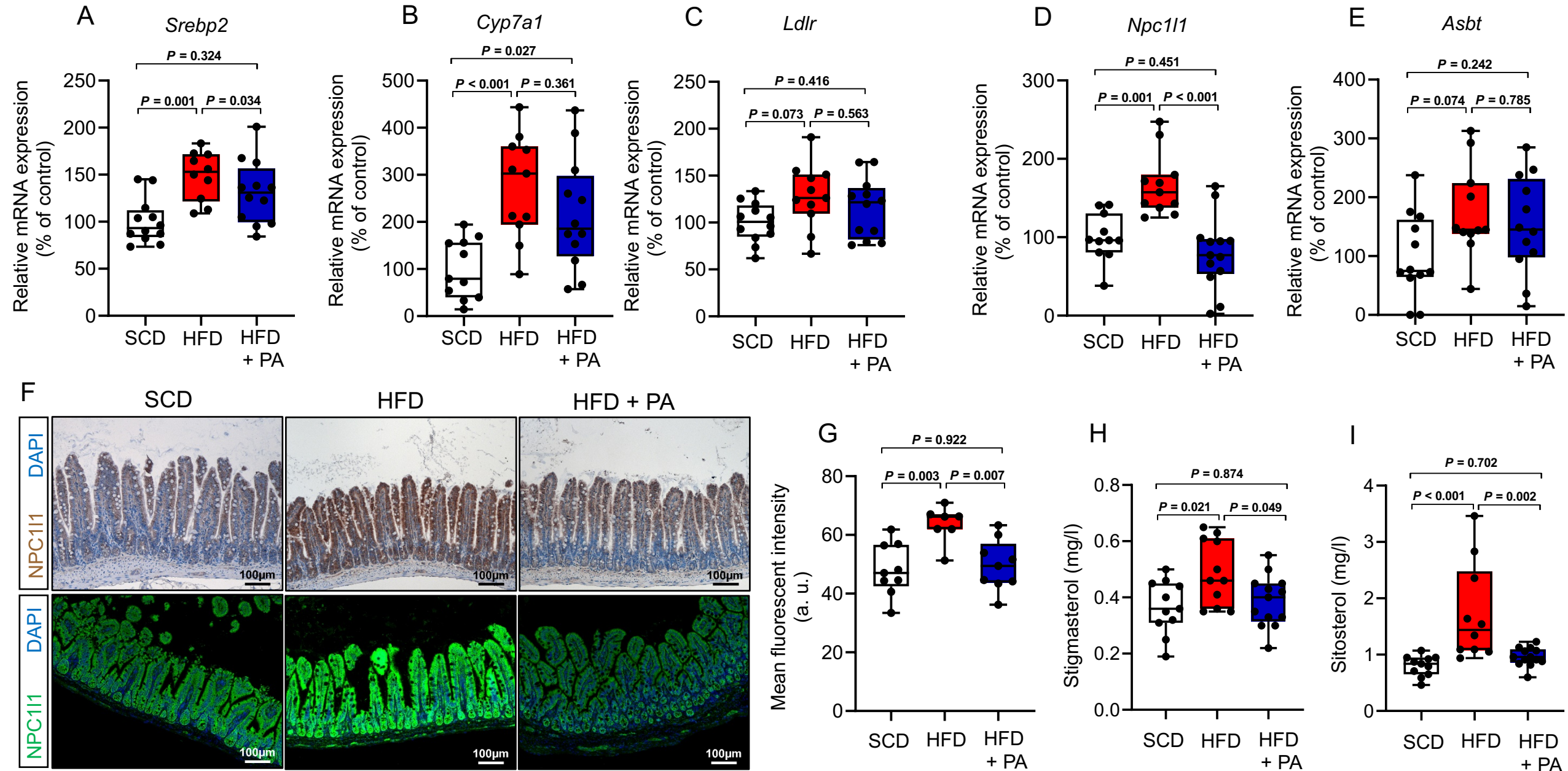


Figure 4

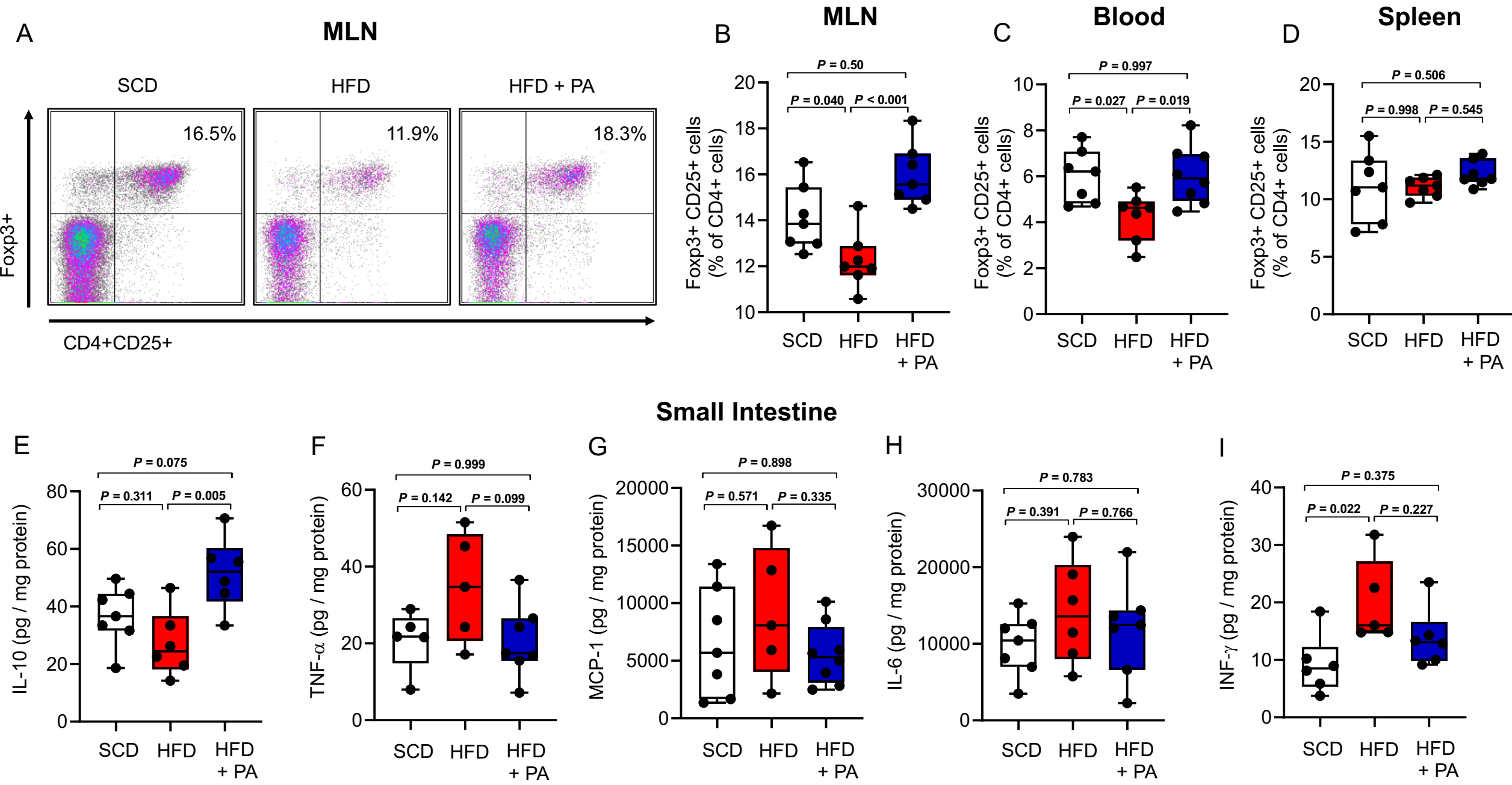


Figure 5

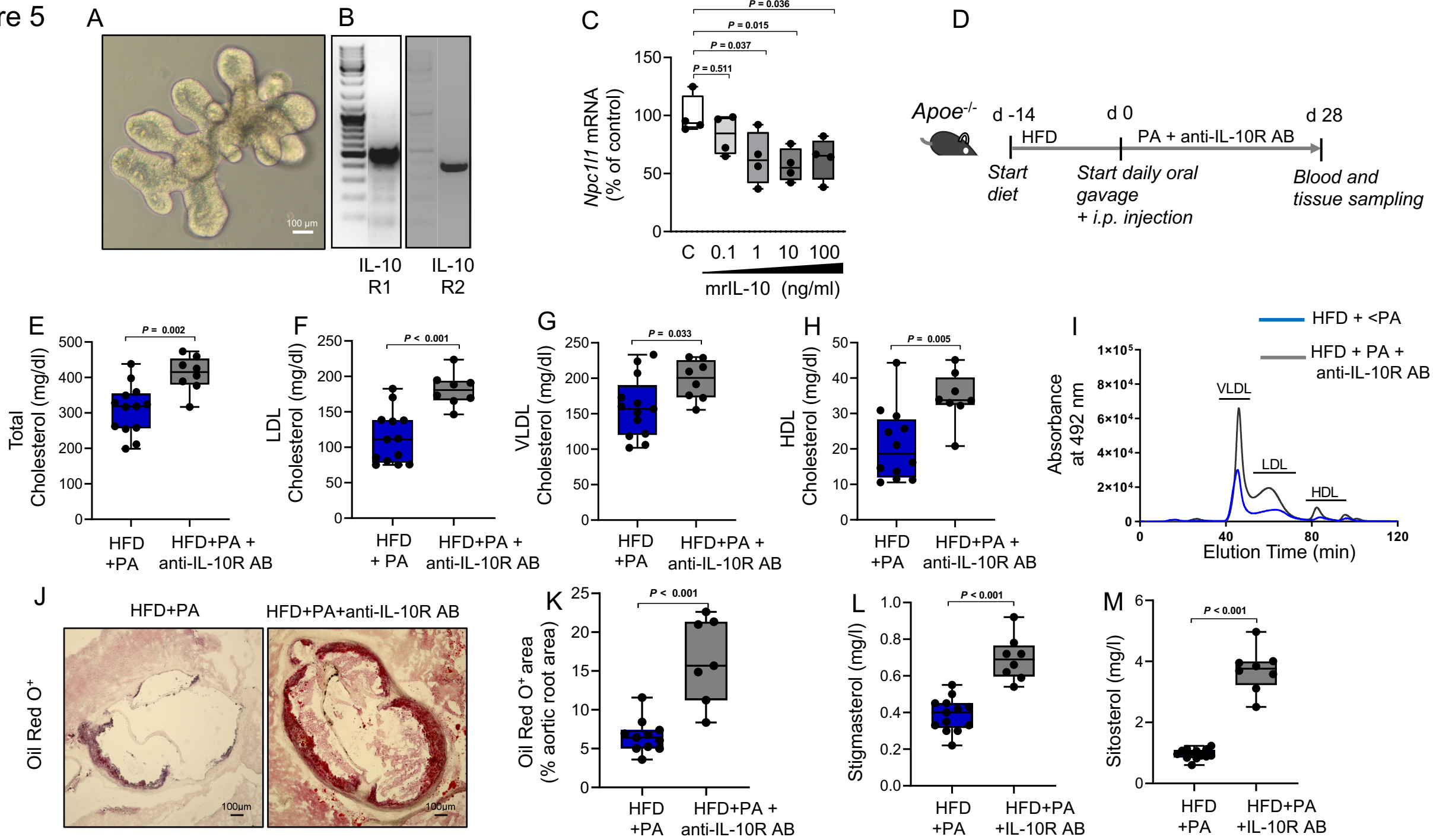
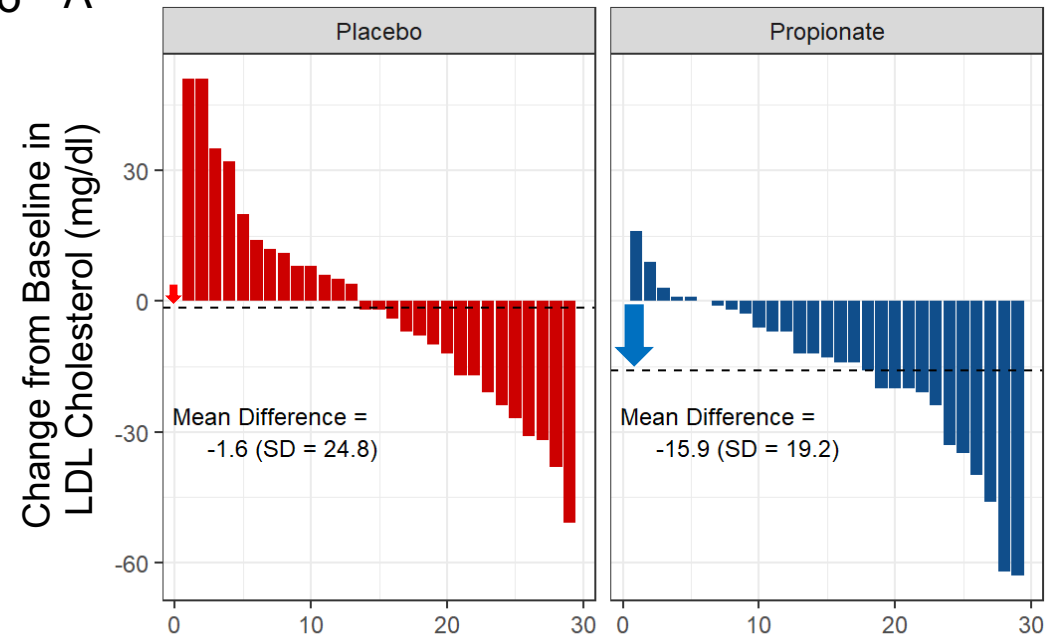
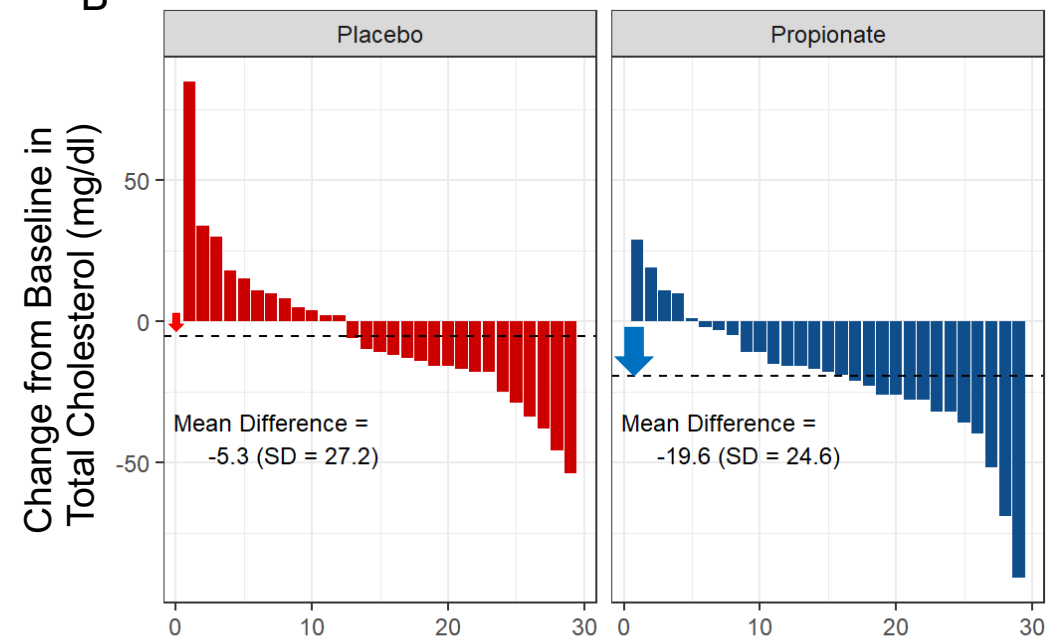


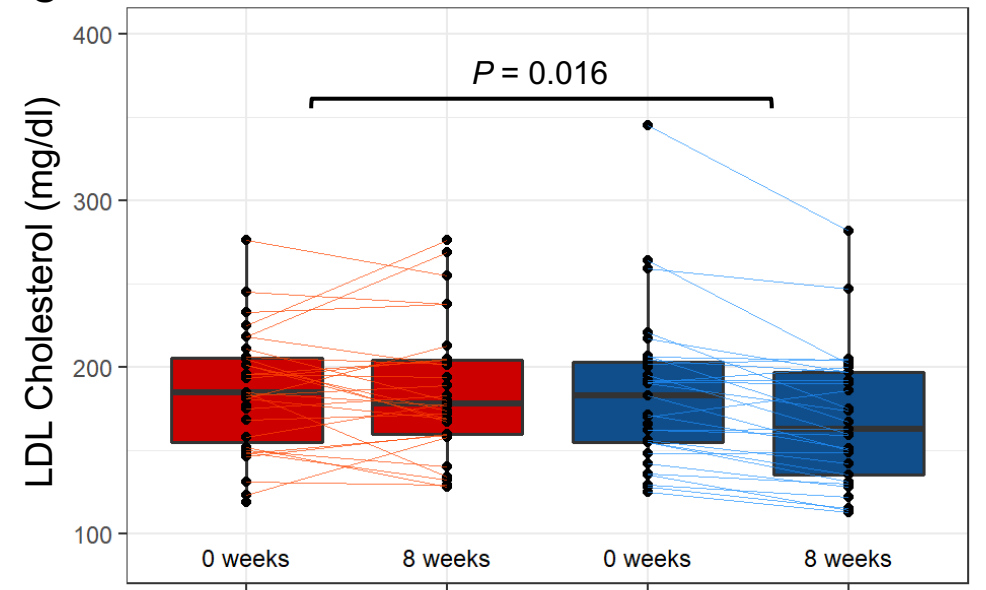
Figure 6 A



B

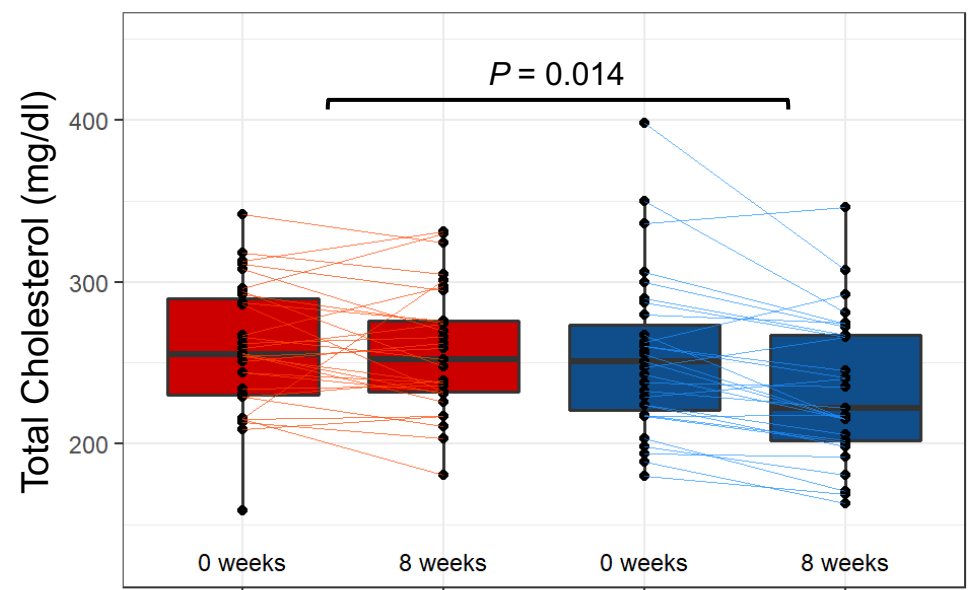


C



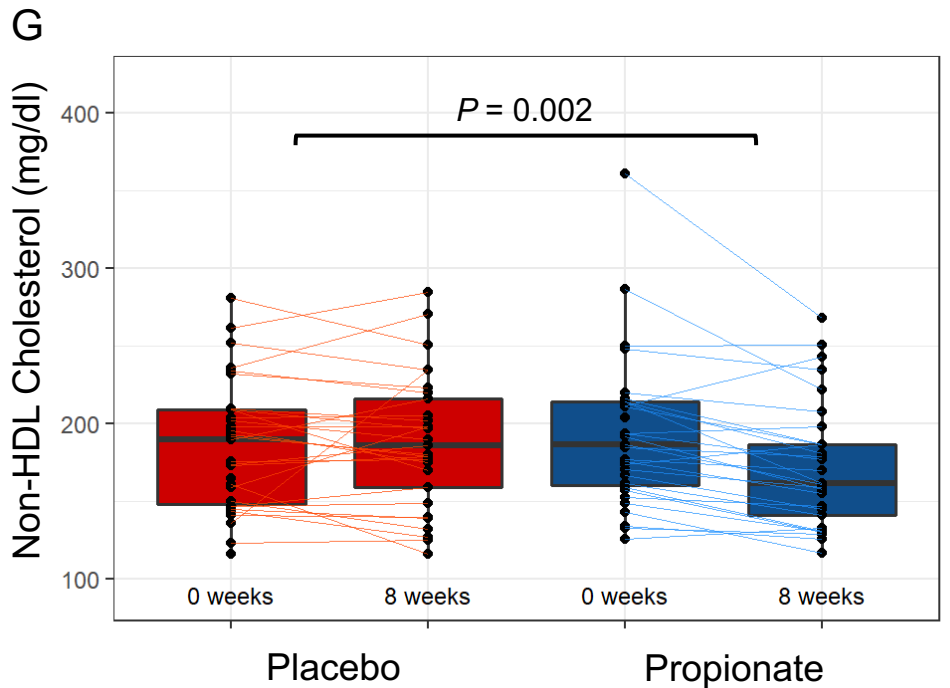
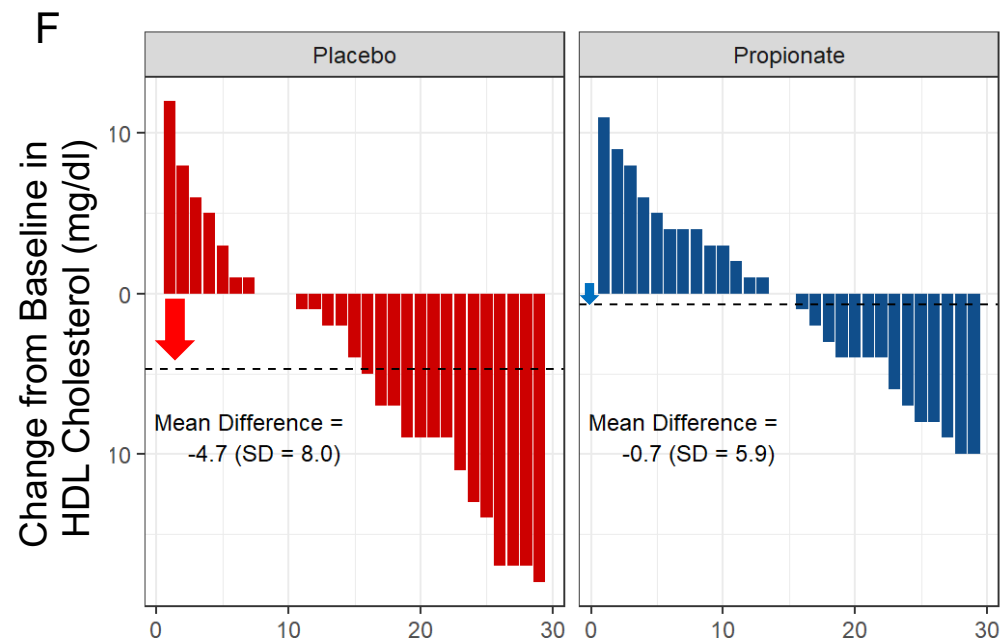
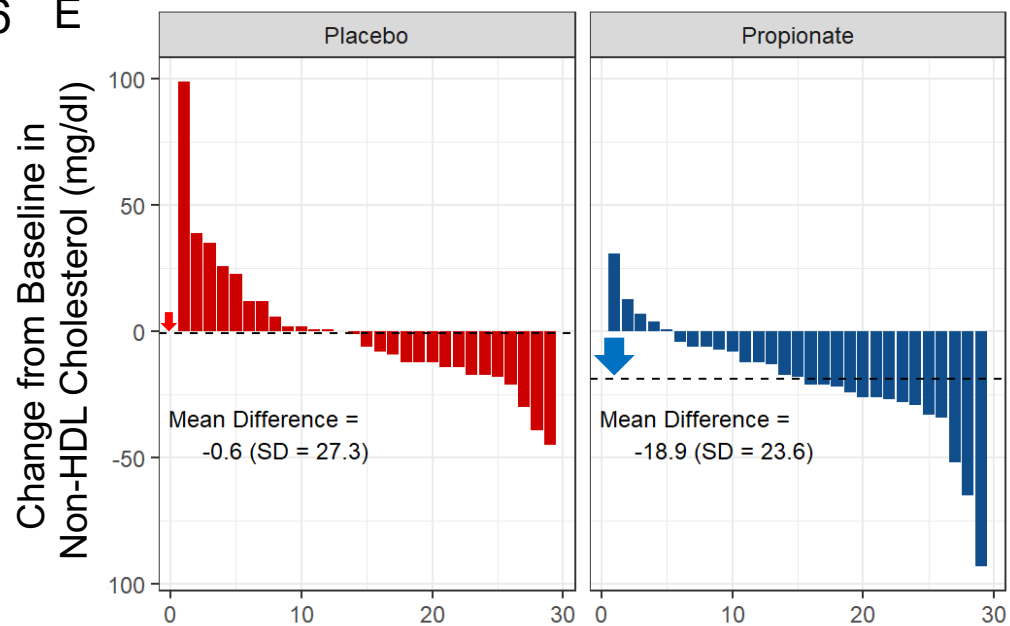
Difference between: Mean (95% CI): -14.32 (-25.81; -2.83)

D

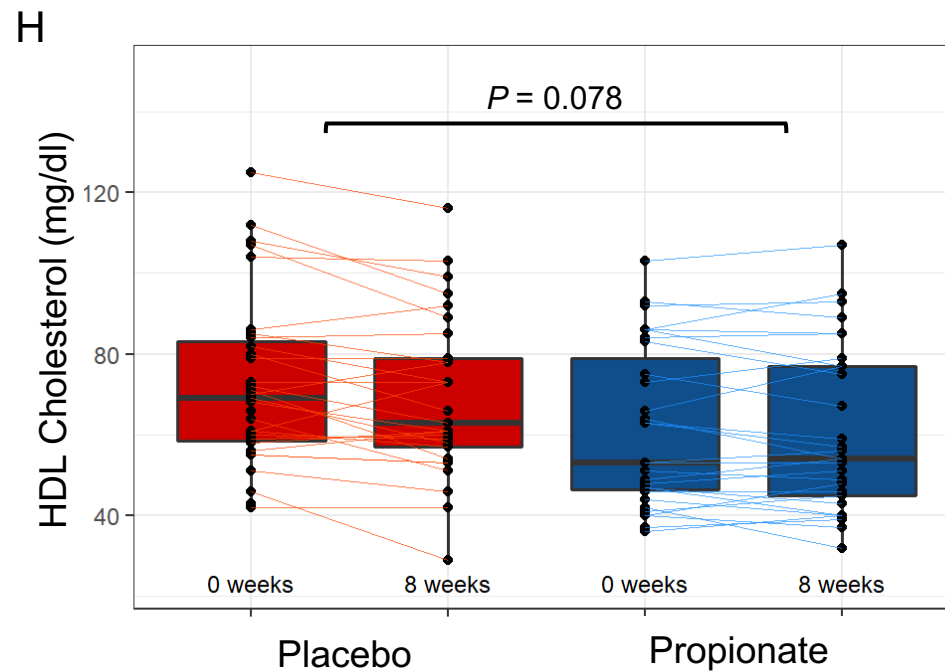


Difference between: Mean (95% CI): -16.68 (-29.85; -3.50)

Figure 6 F

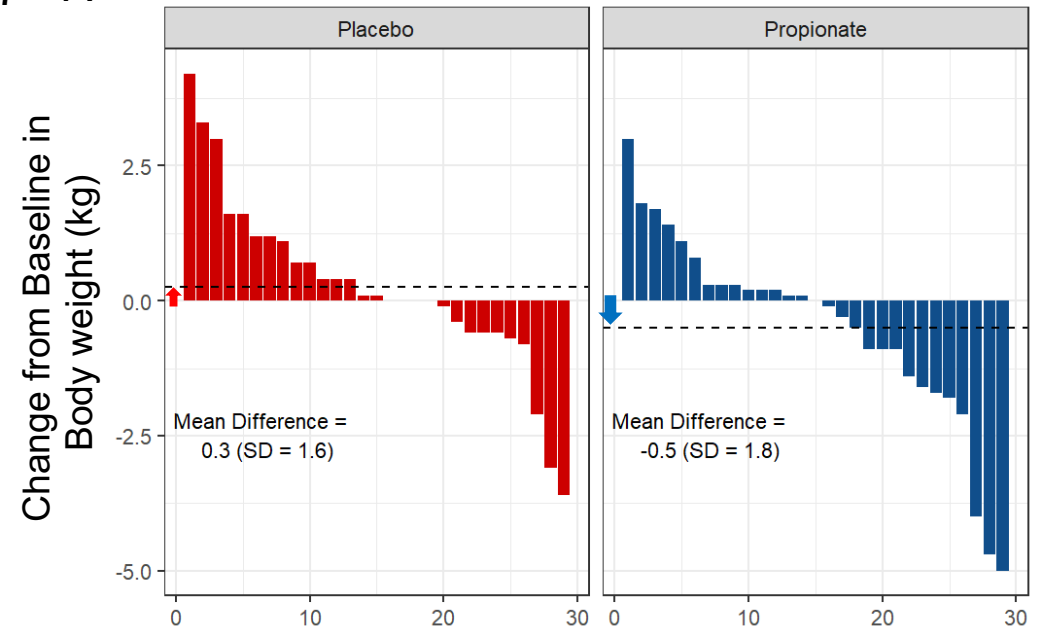


Difference between: Mean (95% CI): -20.77 (-33.60; -7.96)



Difference between: Mean (95% CI): 3.21 (-0.38; 6.80)

Figure 7 A



B

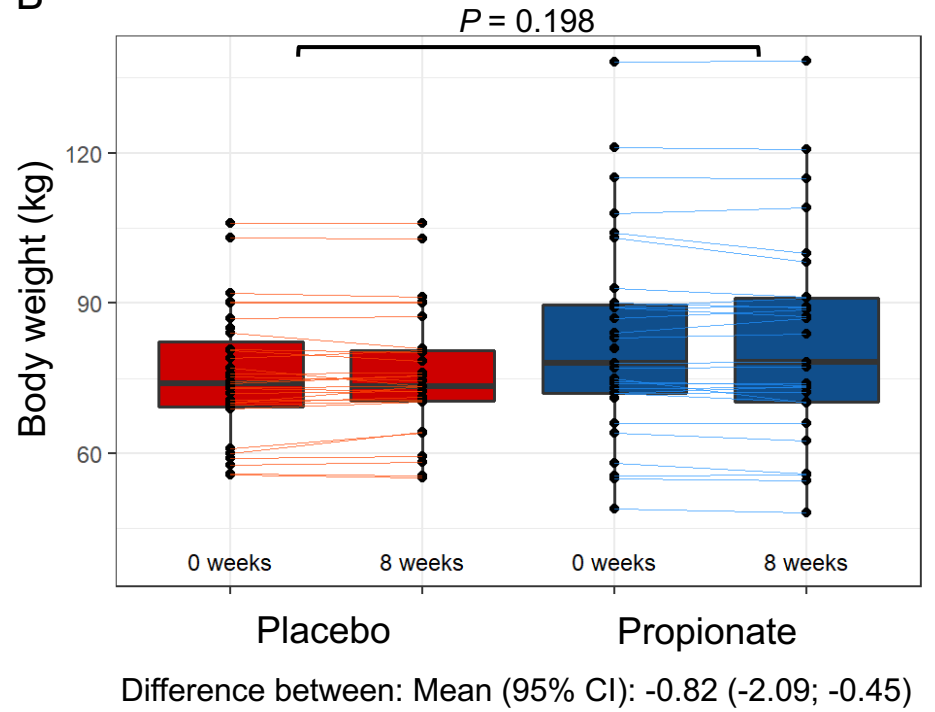


Figure S1

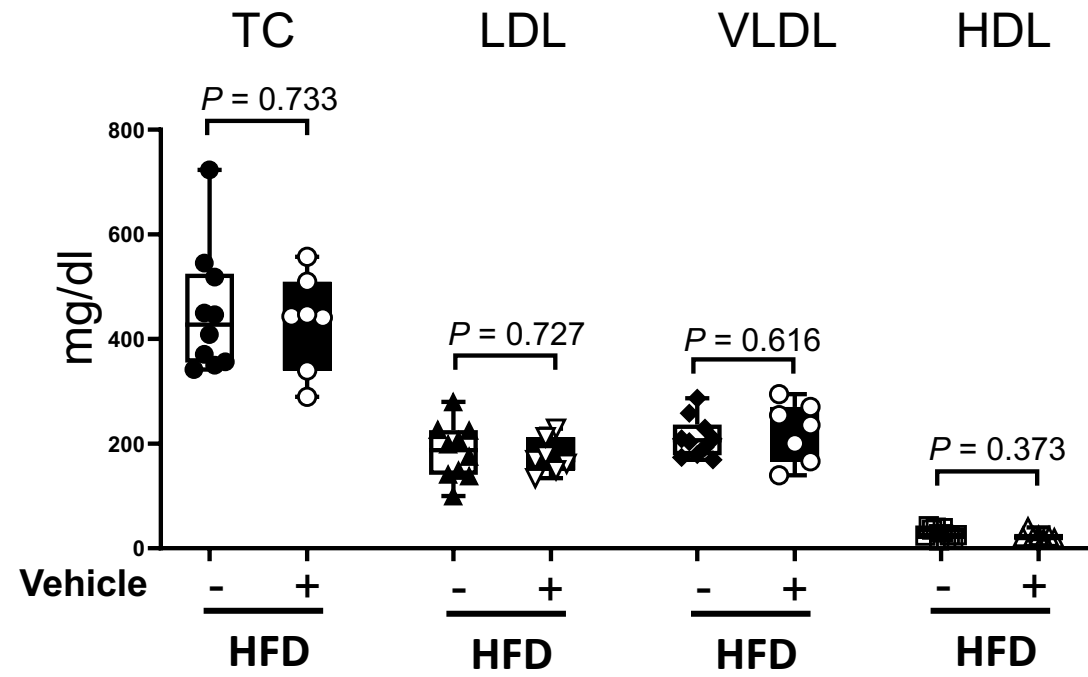
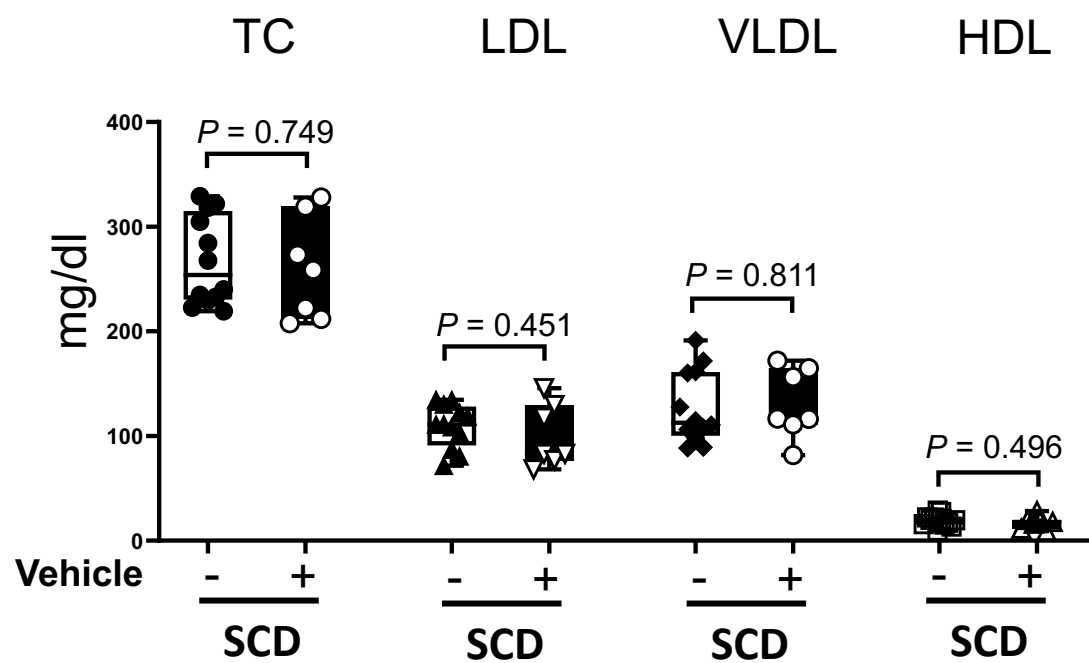


Figure S2

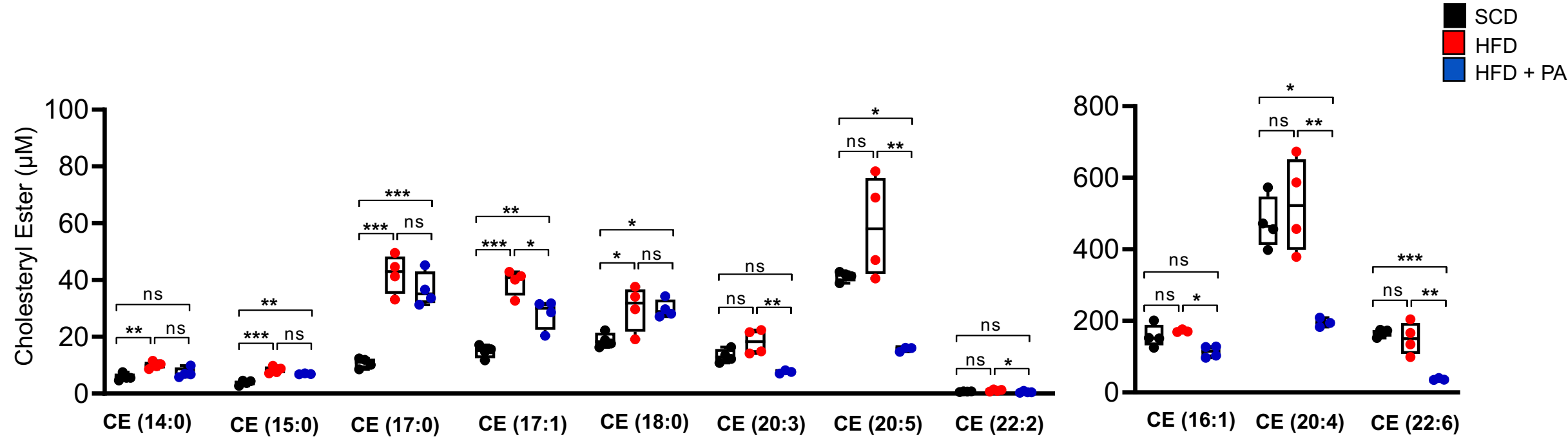


Figure S3

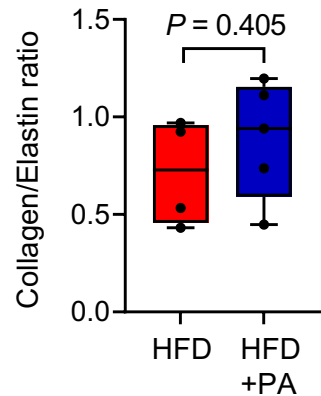
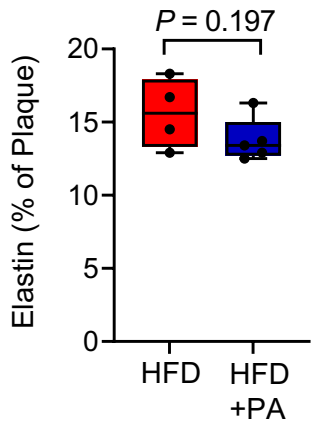
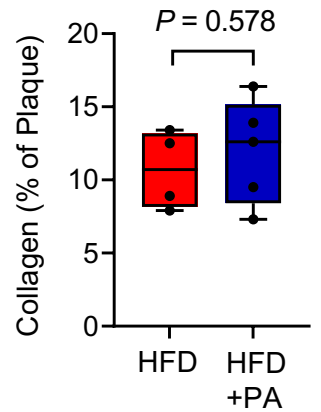
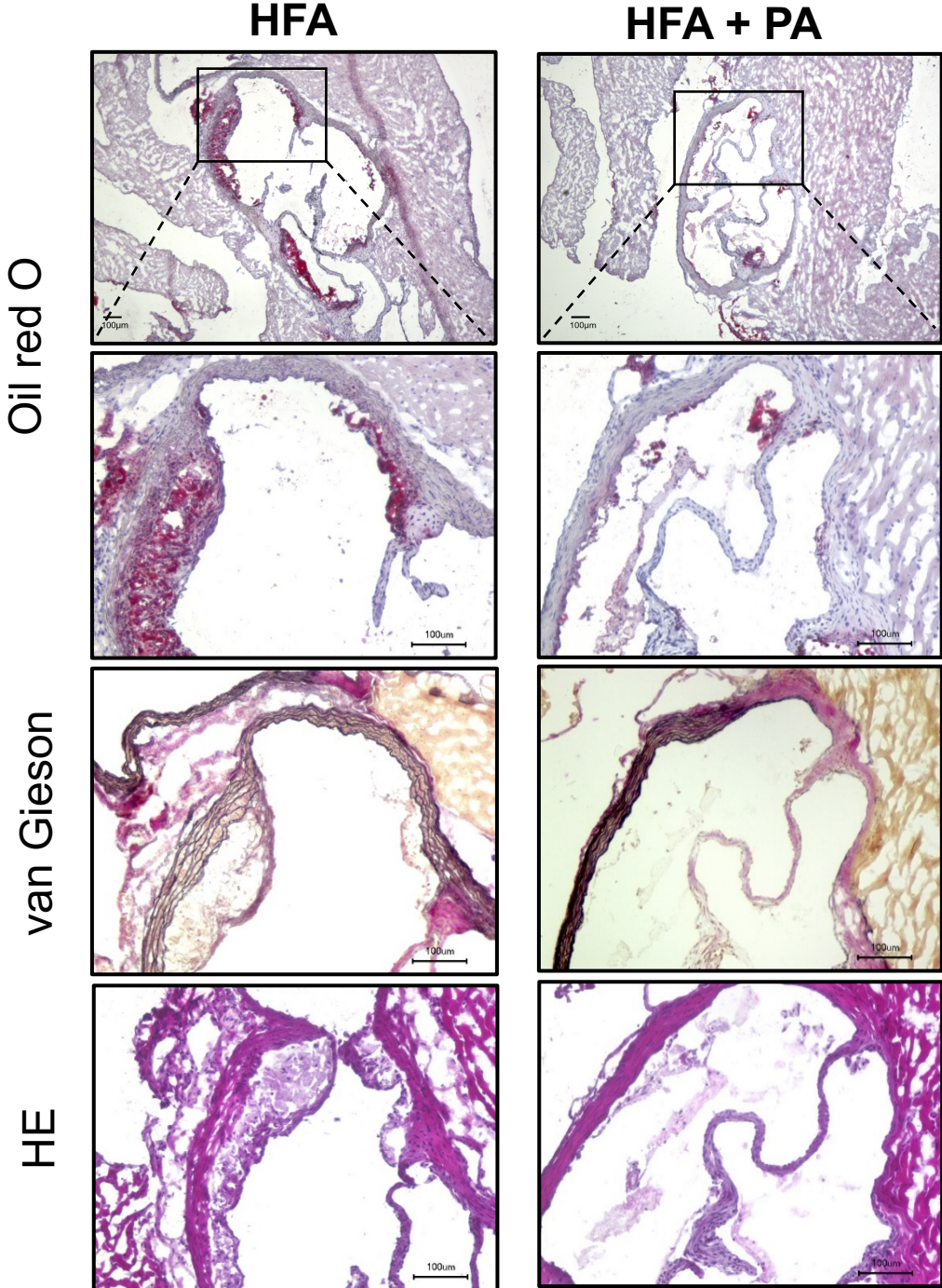


Figure S4

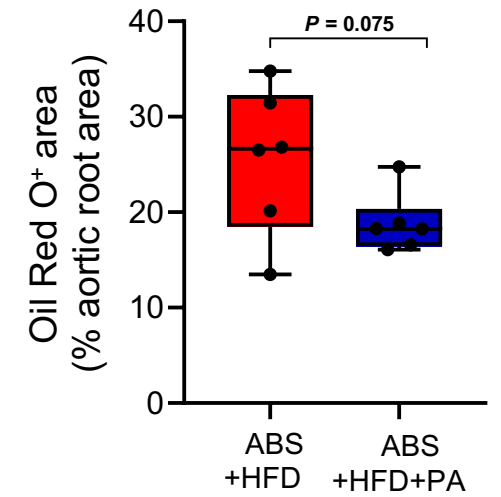
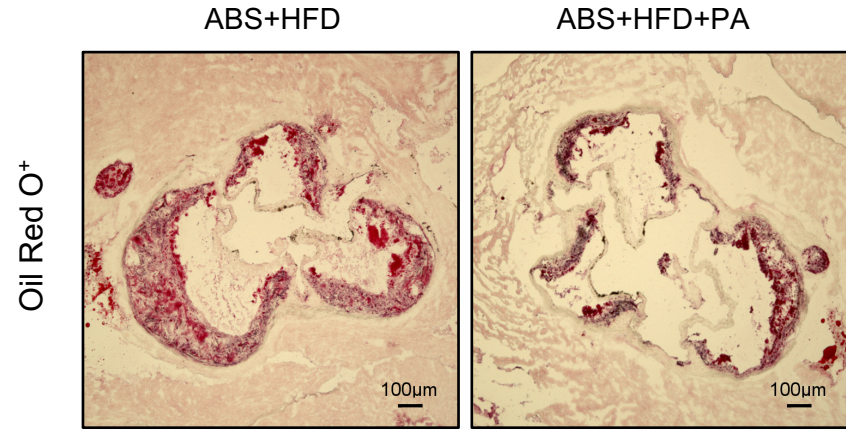
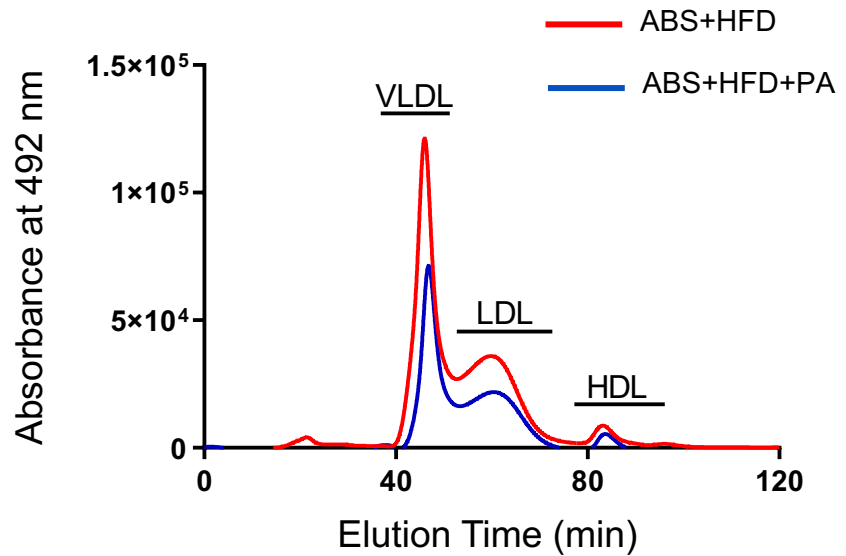
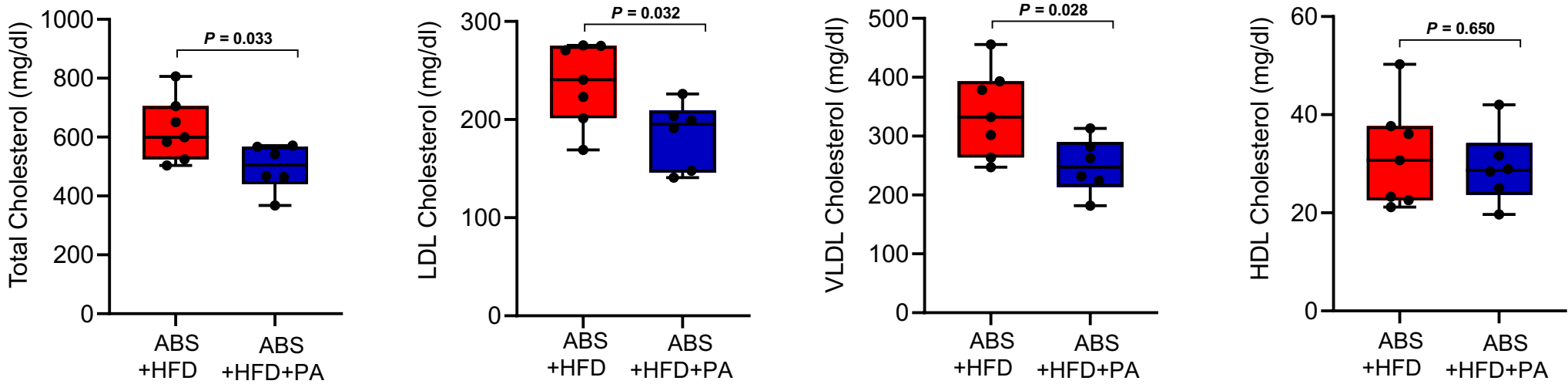


Figure S5

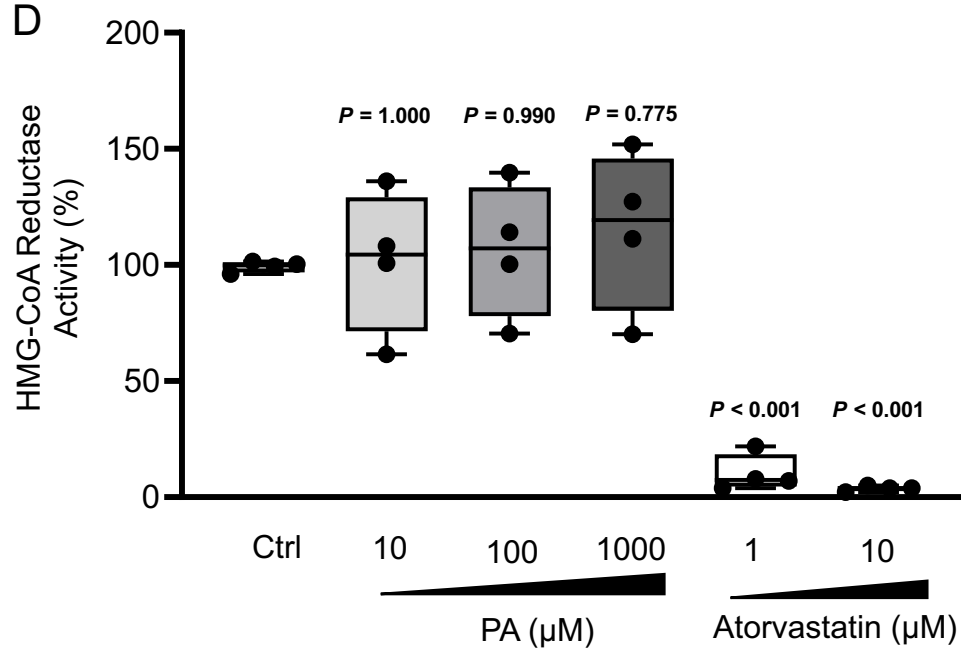
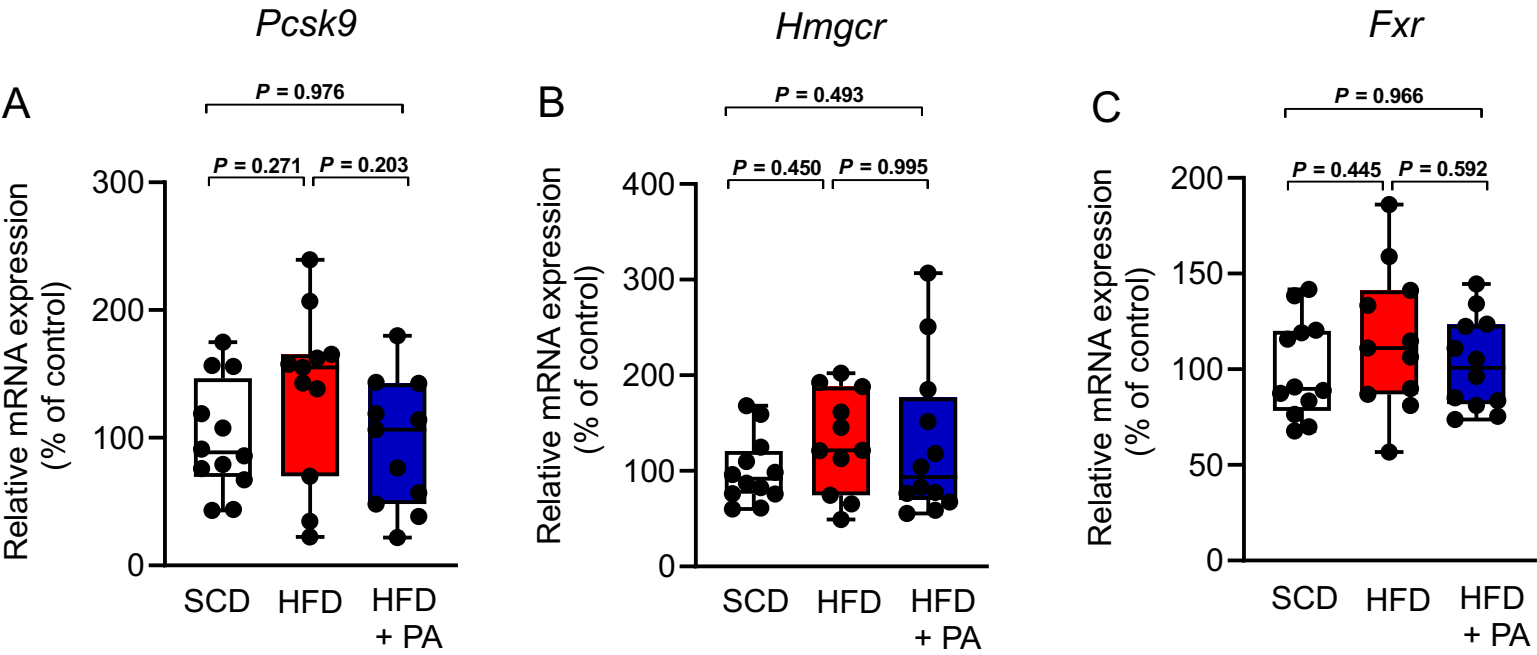


Figure S6

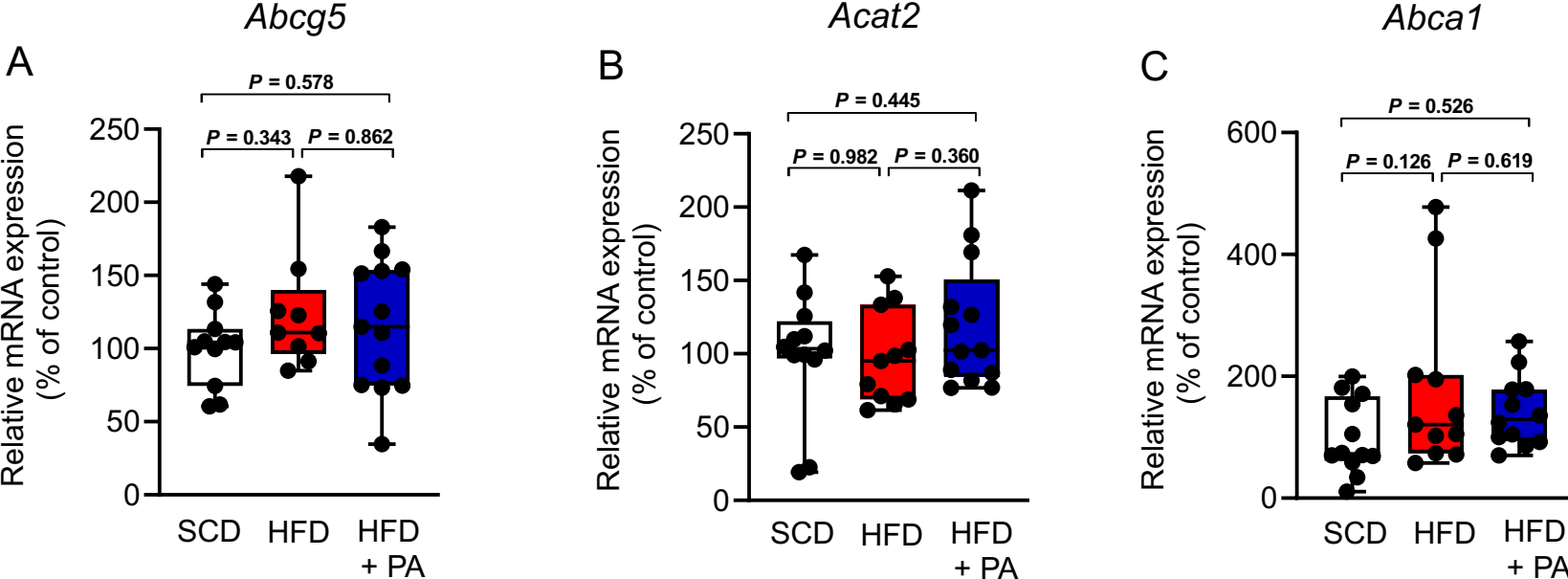


Figure S7

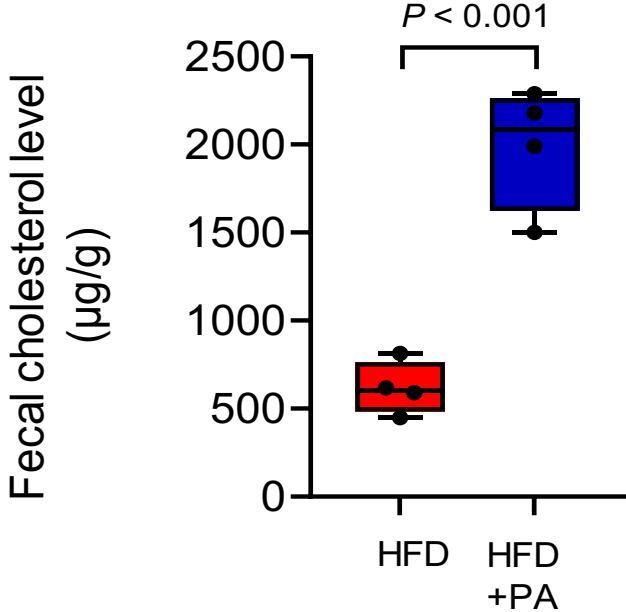


Figure S8

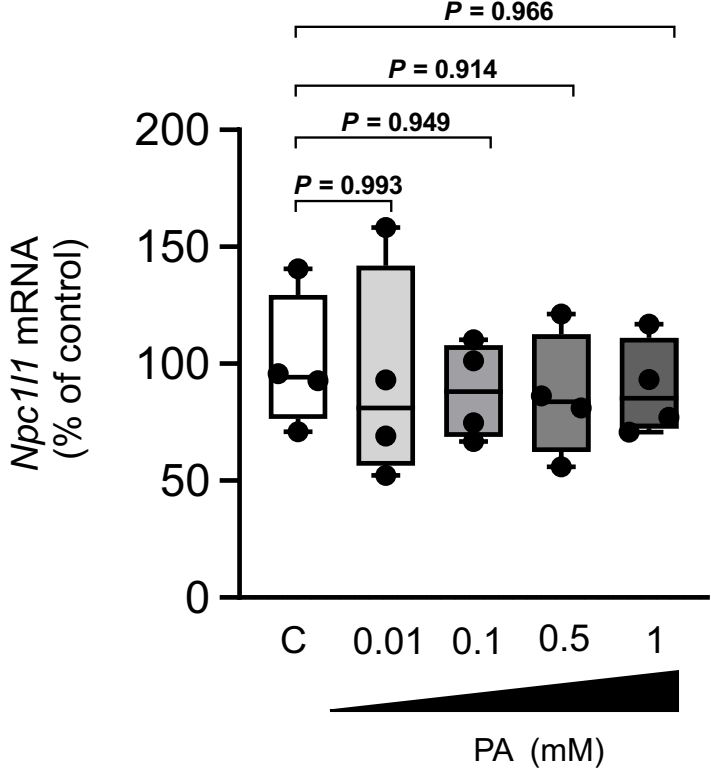


Figure S9

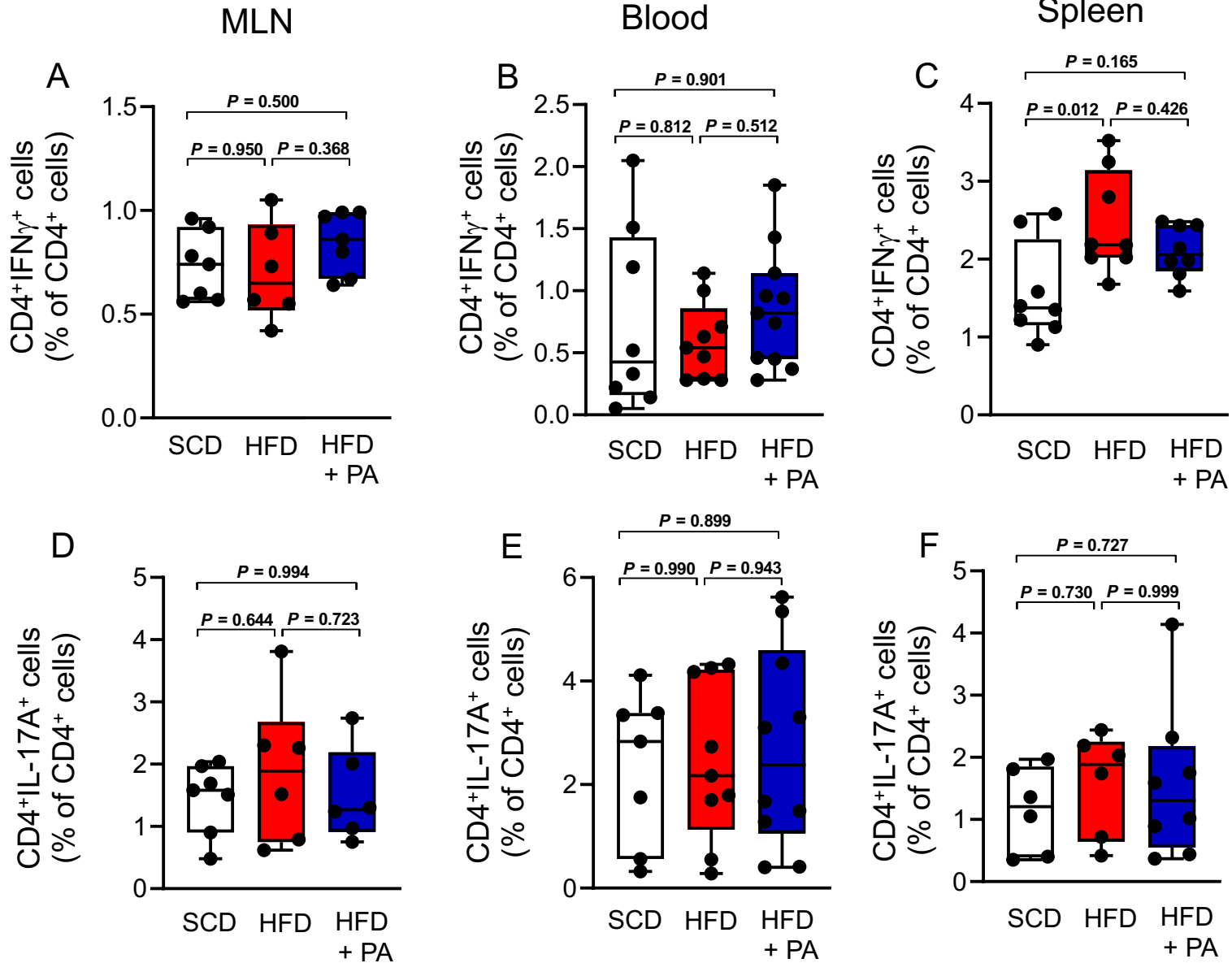


Figure S10

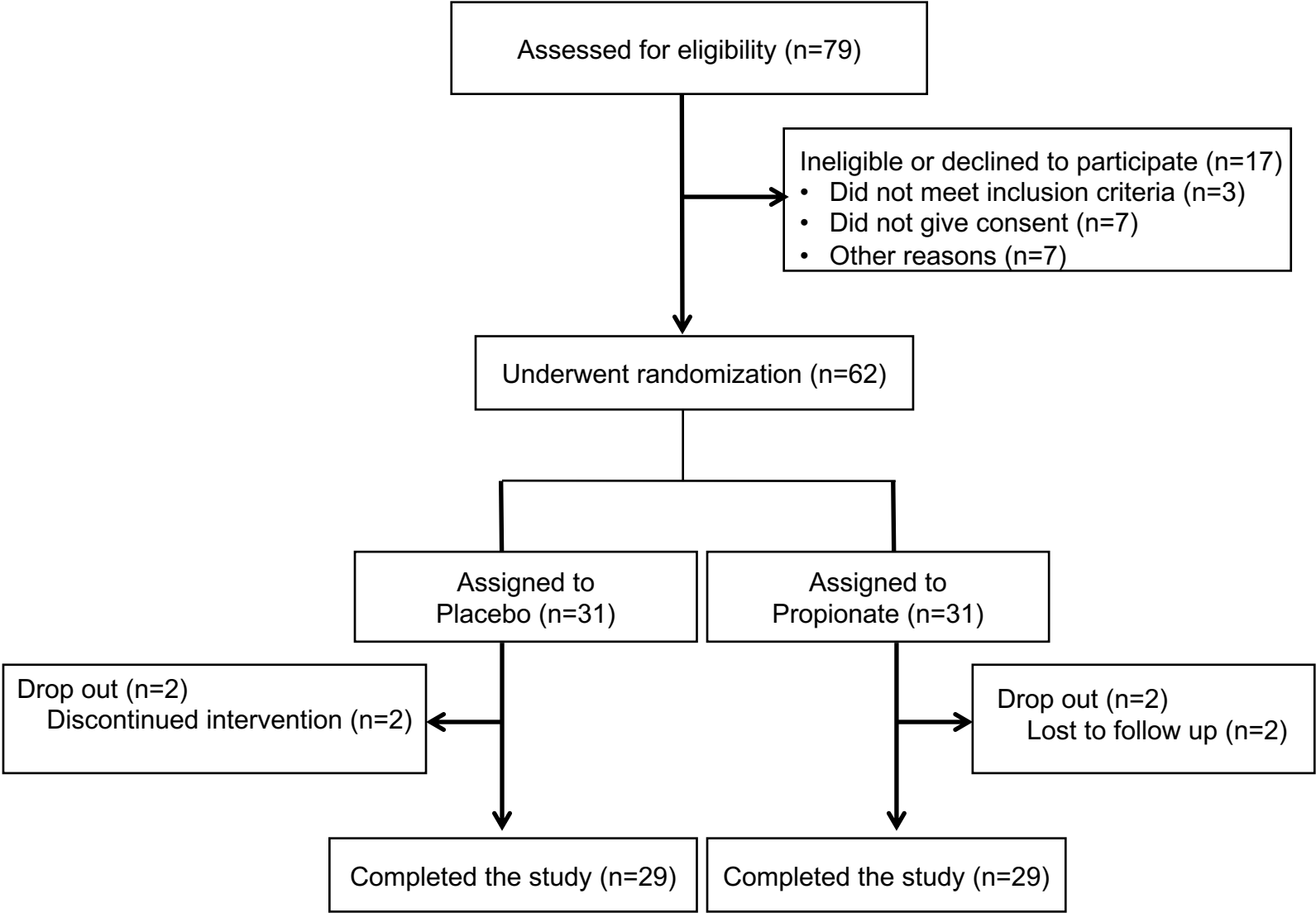


Figure S11

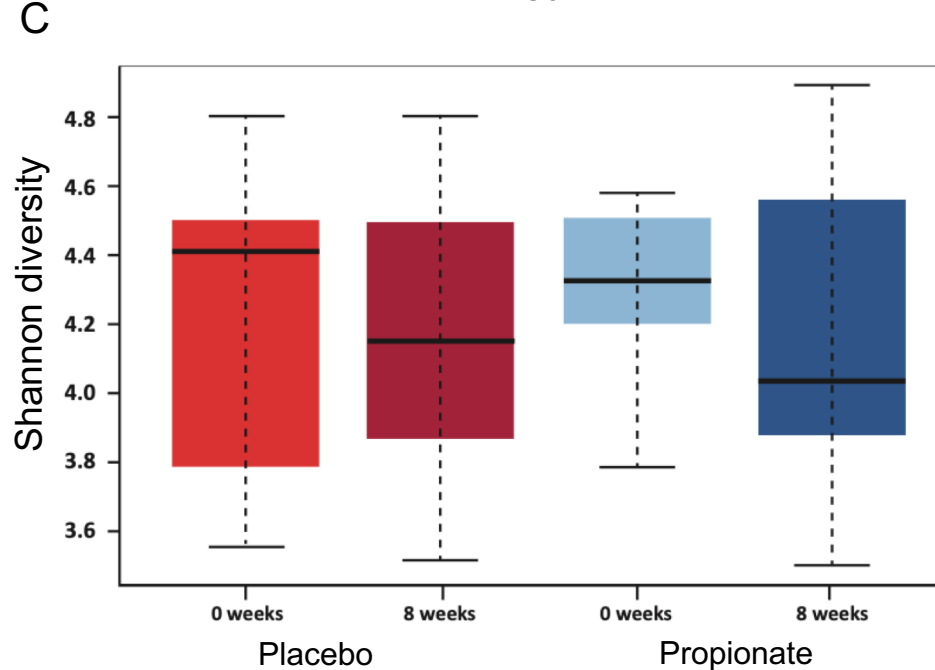
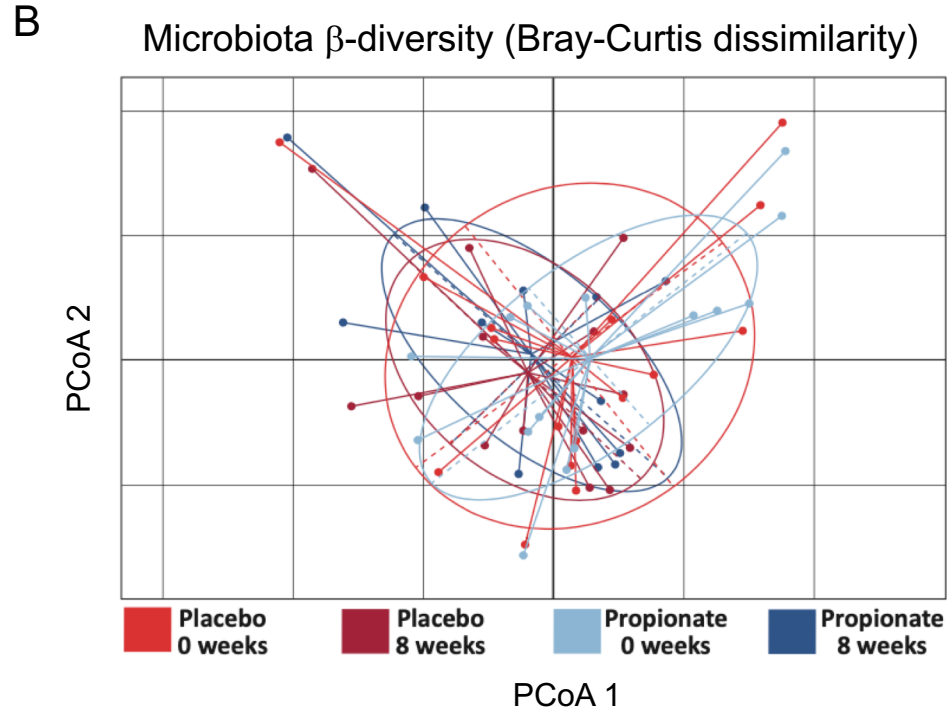
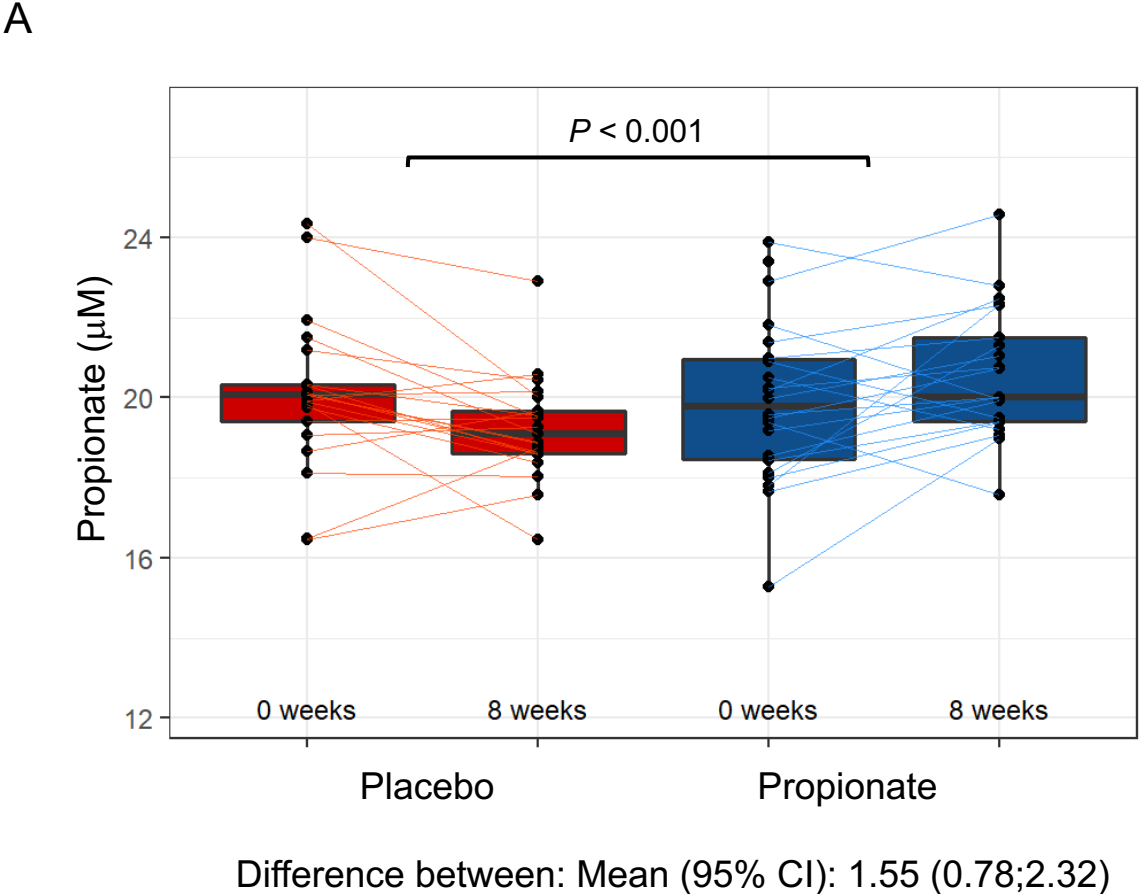


Figure S12

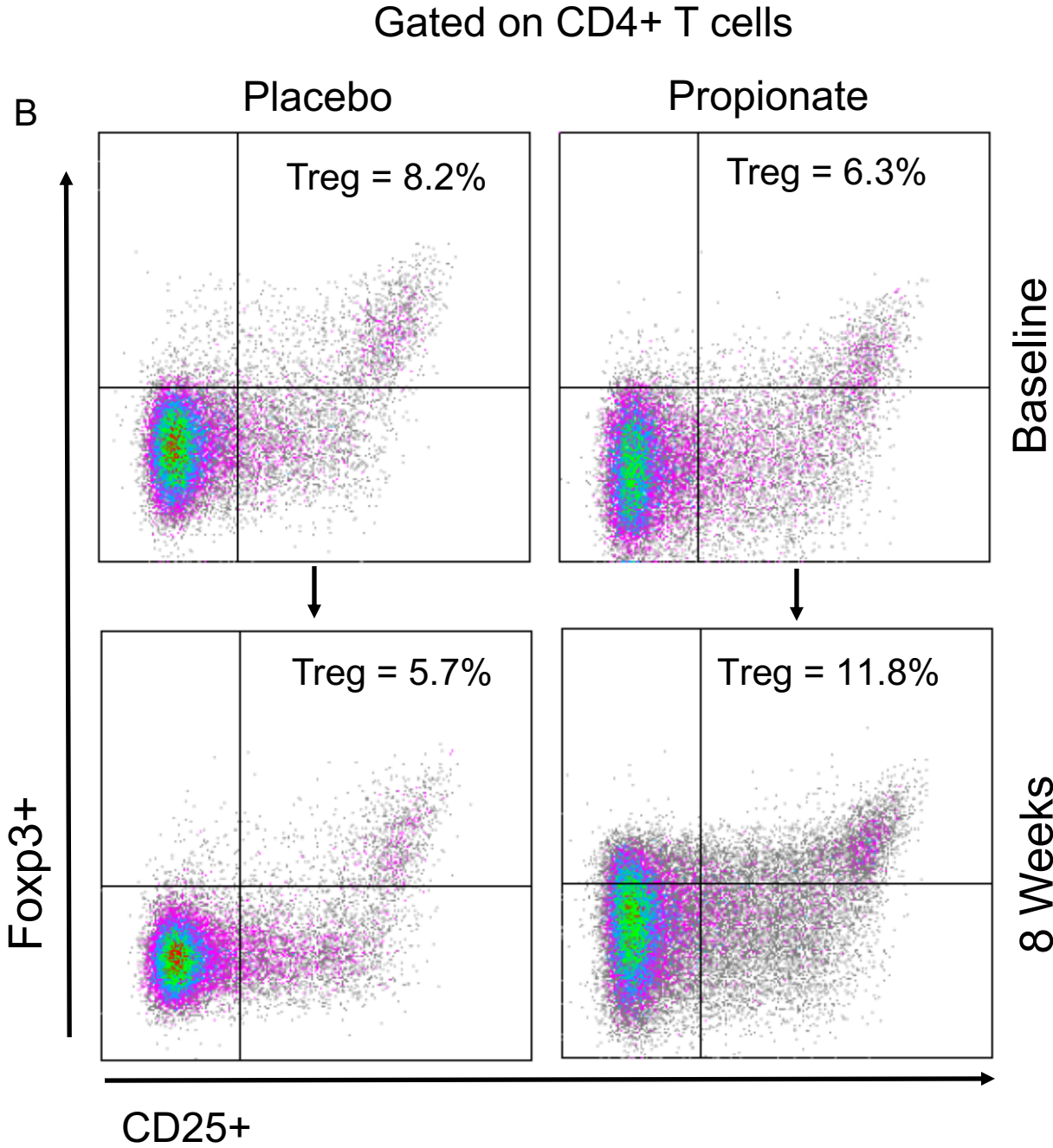
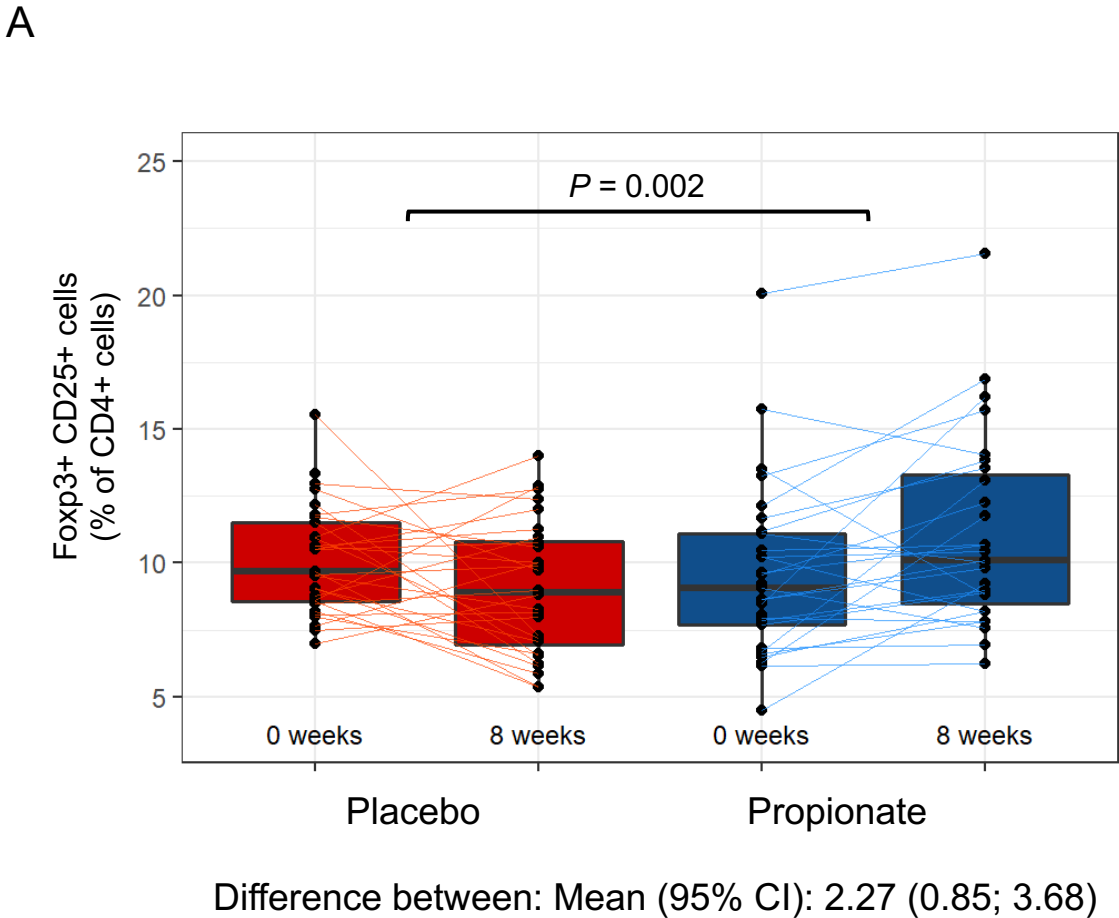
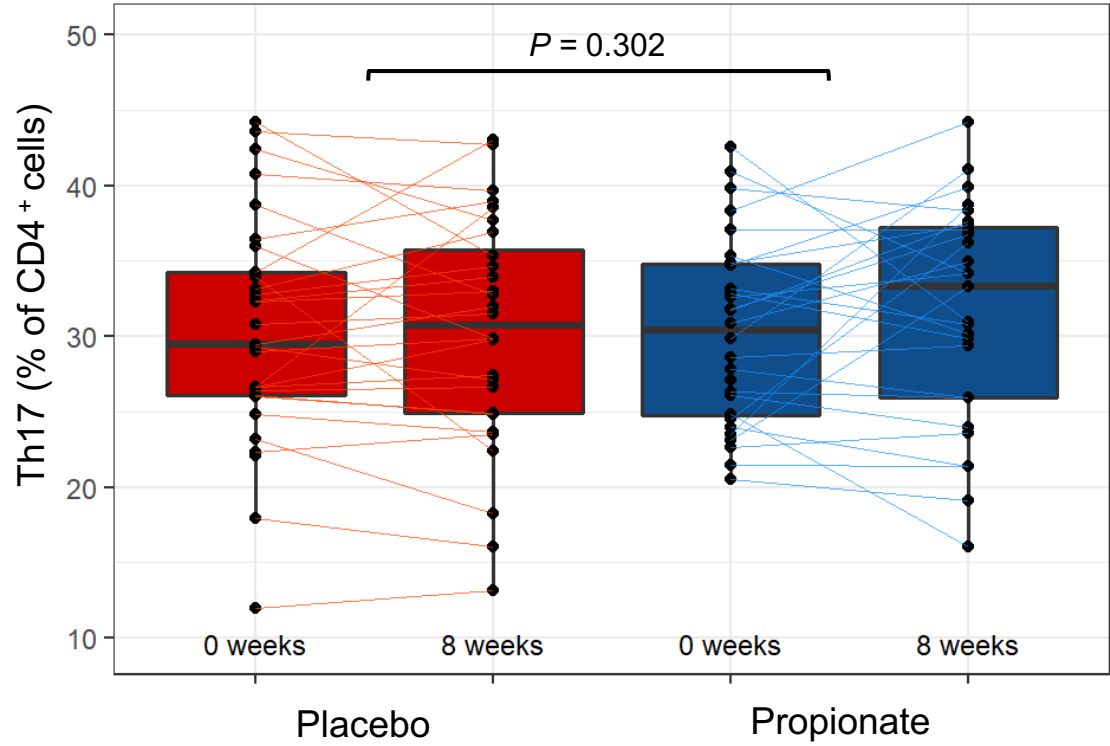


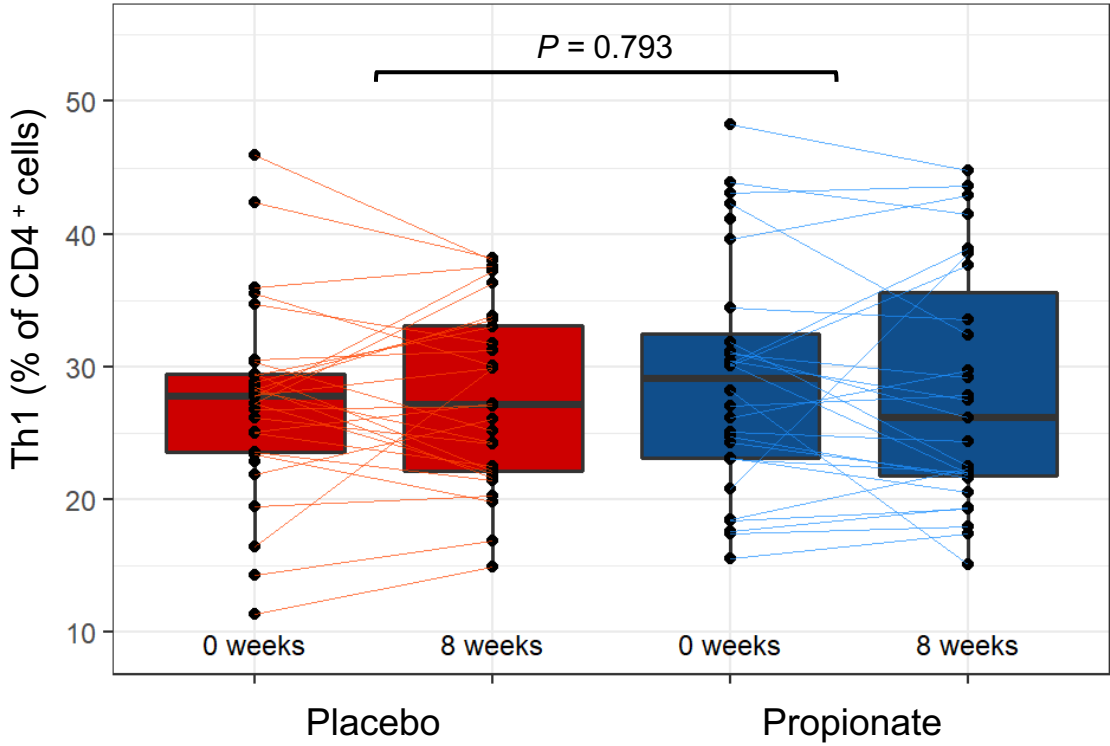
Figure S13

A



Difference between: Mean (95% CI): 1.51 (-1.40; 4.41)

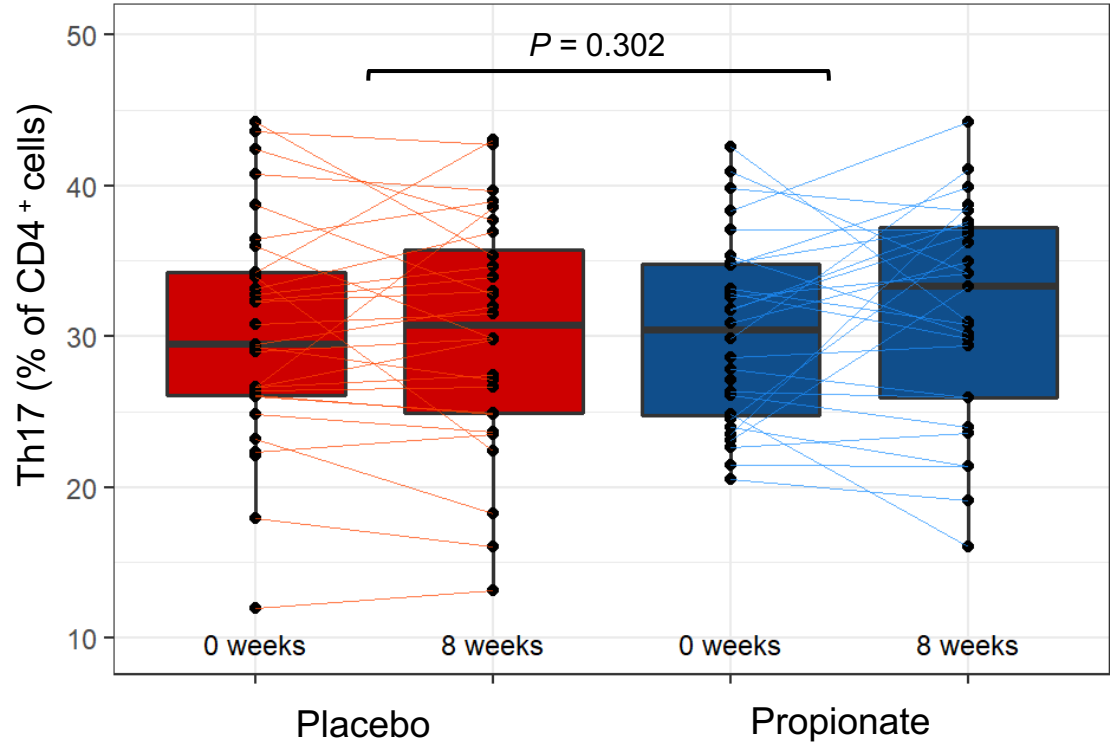
B



Difference between: Mean (95% CI): -0.38 (-3.31; 2.54)

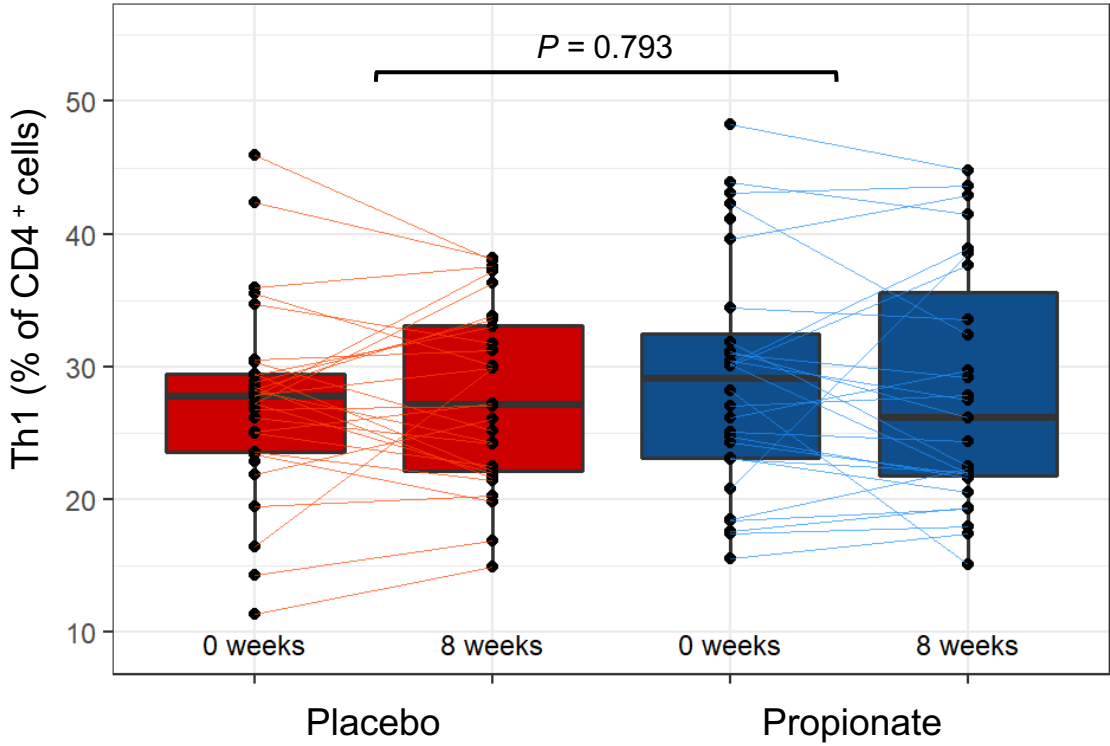
Figure S14

A



Difference between: Mean (95% CI): 1.51 (-1.40; 4.41)

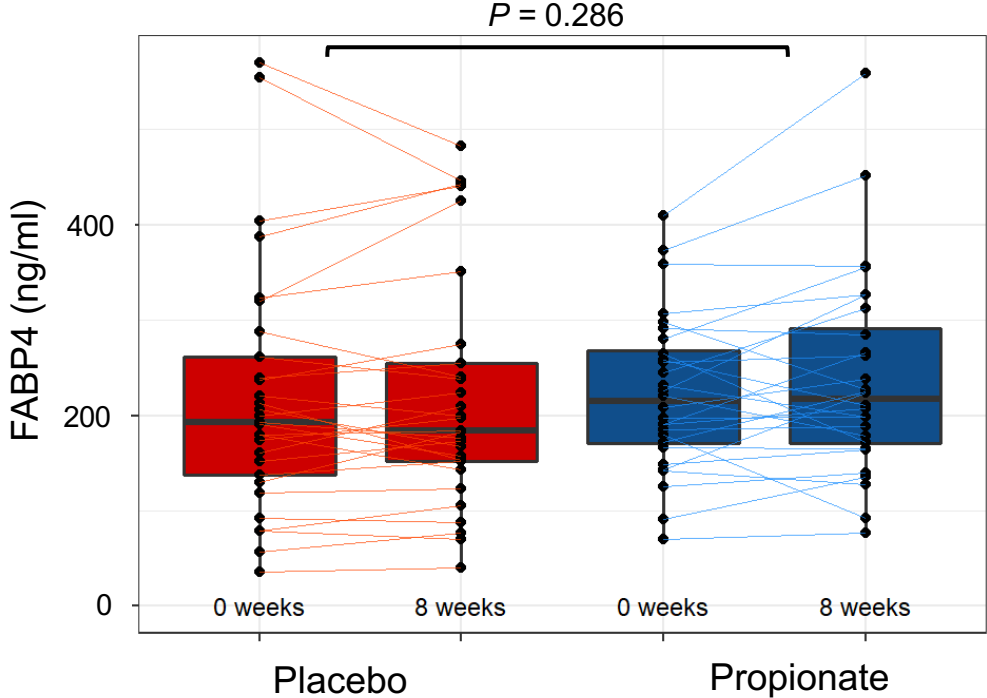
B



Difference between: Mean (95% CI): -0.38 (-3.31; 2.54)

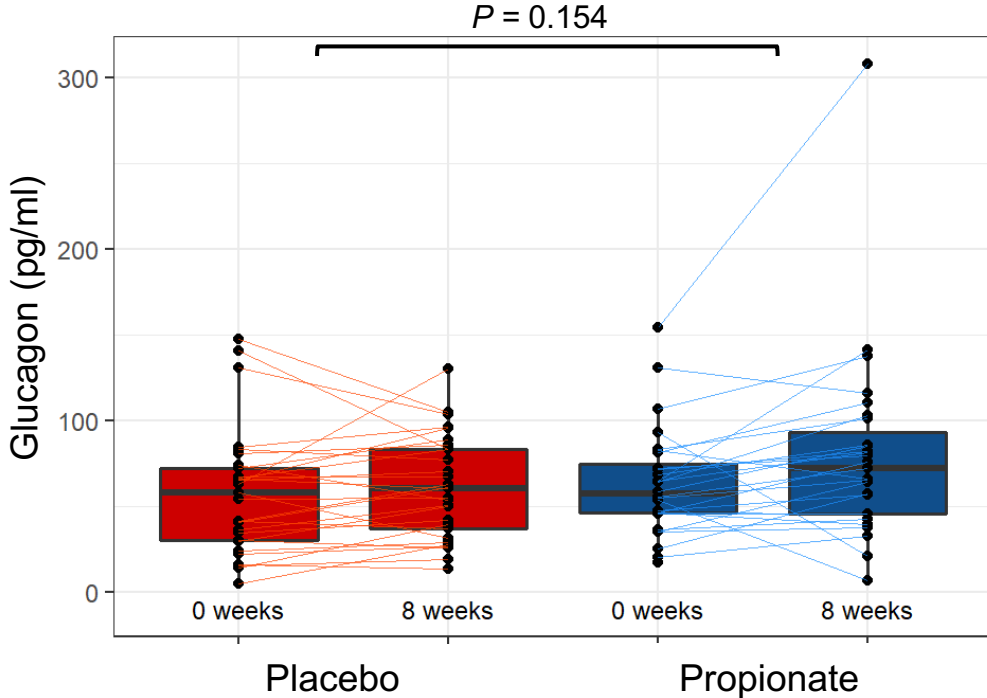
Figure S15

A



Difference between: Mean (95% CI): 146.2 (-126.0; 418.4)

B



Difference between: Mean (95% CI): 12.5 (-4.83; 29.83)

Figure S16

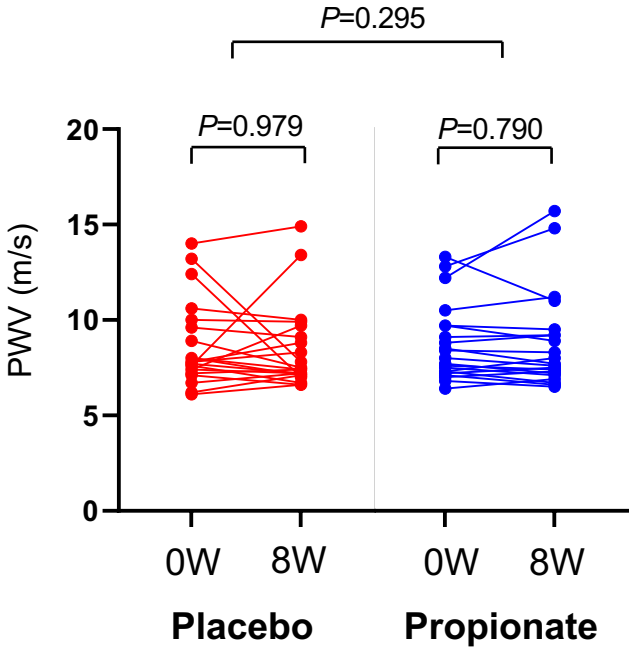
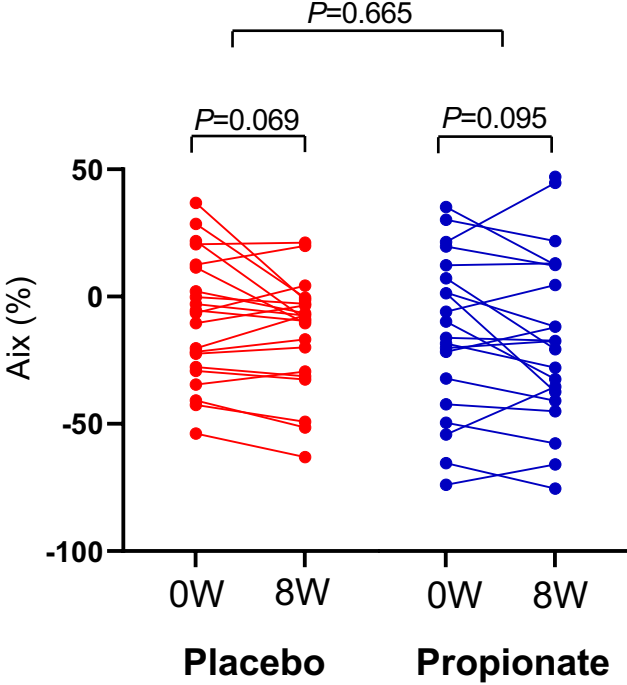


Figure S17

